Plutonium retention in the isosaccharinate – cement system

A. Tasi [a,*], X. Gaona [a,**], Th. Rabung [a], D. Fellhauer [a], J. Rothe [a], K. Dardenne [a],
J. Lützenkirchen [a], M. Grivé [b], E. Colàs [b], J. Bruno [b], K. Källstrom [c], M. Altmaier [a], H. Geckeis [a]

[a] *Karlsruhe Institute of Technology, Institute for Nuclear Waste Disposal, P.O. Box 3640, 76021, Karlsruhe, Germany*
[b] *Amphos 21 Consulting S.L., Passeig de Garcia i Fària, 49-51, 1°-1ª, E08019, Barcelona, Spain*
[c] *Svensk Karnbranslehantering AB, Avd. Låg–och medelaktivt Avfall, Evenemangsgatan 13, Box 3091, 169 03, Solna, Sweden*

ABSTRACT

Uptake of plutonium by Portland cement in degradation stage II was investigated in the presence of α-D-iso-saccharinic acid (ISA) under reducing conditions set by hydroquinone, Sn(II) or $Na_2S_2O_4$. Sorption experiments were performed at log $[Pu]_{in} = 6$ to 9, log $[ISA]_{tot} = 6$ to 2 and with solid to liquid ratios (S:L) of 0.1–$50 \, g \cdot dm^{-3}$. ISA sorbs strongly on cement, causing a significant decrease in the ζ potentials of cement particles above log $[ISA]_{tot} \geq 3.5$ at S:L $\leq 4 \, g \cdot dm^{-3}$. Sorption of Pu significantly decreases above log $[ISA]_{tot} \geq 4.5$ due to the competing formation of aqueous Ca(II)–Pu(IV)–ISA complexes. The increased retention of Pu observed above ~25% of surface coverage by ISA is attributed to the co-adsorption of Pu(IV) with ISA. The impact of the order of addition of individual components on Pu sorption kinetics can be on the scale of several years.

1. Introduction

Cementitious materials are widely used both for the conditioning of radioactive waste and for engineering applications in underground repositories for the disposal of low- and intermediate-level radioactive waste (L/ILW), as well as for high-level radioactive waste (HLW). In the post-closure period of these facilities, water intrusion may induce various degradation processes. Hydrated cement phases will buffer the pH and concentrations of certain metal ions (*e.g.* Ca^{2+}, Al^{3+}, etc.). Three main stages are described for the degradation of cement by the interaction with inflowing groundwater. In stage I, the pore water composition is buffered by the dissolution of Na and K oxides/hydroxides, which result in high alkali concentrations ([Na] ≈ 0.1 M, [K] ≈ 0.2 M) and pH (≈13.3). Stage II is dominated by the dissolution of portlandite, $Ca(OH)_2(s)$, which buffers the pH (≈12.5) and calcium concentration ([Ca] ≈ 0.02 M) in the pore water. In stage III and after the complete dissolution of portlandite, pore water composition is controlled by the non-congruent dissolution of calcium silicate hydrate (C–S–H) phases (pH ≈ 12.5 → 10). Anaerobic corrosion of the iron present in the repository (*e.g.* steel containers) and consequent generation of $H_2(g)$ will impose strongly reducing conditions, with (pe + pH) values set close to the lower borderline of the stability field of water over a long time-scale (Duro et al., 2014; SKB, 2008).

Plutonium is a relevant radionuclide in the long-term safety assessment of underground repositories for nuclear waste. A large inventory of [239]Pu is present in high level radioactive waste (HLW) as a component of spent fuel. Although generally not abundant in L/ILW, plutonium may also contribute to the long-term risk of repositories for such wastes (SKB, 2008). In addition to the long half-life of [239]Pu (t½ [239]Pu $2.41 \cdot 10^4$ a), the possible simultaneous co-existence of different oxidation states in aqueous solutions represents significant challenges both for experimental investigations and for the predictive assessment of its chemical behavior. Under the hyperalkaline and reducing environment of underground repositories in the presence of cement, Pu(IV) is expected to predominate with minor contributions of Pu(III) (Tasi et al., 2018c).

C–S–H phases are among the main components of hydrated cement. They exhibit a large surface area ($148 \, m^2/g$ at Ca:Si ratio of ~1.7 (Tits et al., 2006)) and are considered to be the most important sink for actinide ions in cementitious materials (Ochs et al., 2016; Wang et al., 2009; Wieland, 2014). The available literature data on the uptake of plutonium by cement and/or C–S–H phases is rather limited. Experimental studies on this system are complicated by a number of requirements, such as strict control of the Pu redox state, proper phase separation procedures to avoid the artificial contributions of Pu(IV) colloids during the determination of [Pu], or the need of using sufficiently low Pu concentrations to be undersaturated with respect to the

---

* Corresponding author.
** Corresponding author.
E-mail addresses: agost.tasi@kit.edu (A. Tasi), xavier.gaona@kit.edu (X. Gaona).

low solubility of $PuO_2(am,hyd)$ (log ($[Pu]_{tot}/M$) ≈ −11).

The sorption of Pu on concrete and mortar (among other repository-relevant materials) was studied in the context of the performance assessment concerning extension of the low-level waste repository at Rokkasho-Mura (Baston et al., 1995). Sorption experiments were performed in N_2-gloveboxes, using [236]Pu with an initial concentration of $(5 \pm 1) \cdot 10^{-12}$ M, solid-to-liquid ratios (S:L) of 2 or 20 g dm^{-3} and in the absence of redox buffers. Phase separation was achieved by different centrifugation and filtration (0.45 µm and 30000 Da MWCO filters) approaches. The authors reported high values for the distribution ratio of Pu in their concrete and mortar samples: $(1.4–6.4) \cdot 10^6$ dm^3 kg^{-1}. A sorption model was also developed assuming the uptake of Pu(V) by the silanol groups of the cement phase. The oxidation state of Pu was not determined experimentally but defined on the basis of redox potential measurements in the original pore water solutions (270 mV vs. SHE at pH 12.2 and 12.5). In the absence of a strong redox buffer in solution, experimental E_h values can be highly deceptive and it is therefore a likely hypothesis that the strong uptake is rather attributed to the sorption of Pu(IV). Due to their high thermodynamic stability, it is also possible, that surface complexes of tetravalent Pu (or Np) form even at relatively high E_h values (see e.g. (Banik et al., 2016; Marsac et al., 2015)).

Bayliss and co-workers investigated the uptake of Pu(IV) by cement with different compositions and the Nirex Reference Vault Backfill (NRVB), a cement-based backfill material considered in a conceptual UK geological disposal facility for nuclear waste (Bayliss et al., 1996, 2000). Experiments were performed at pH ≈ 12.6 in the absence of redox buffers and with $[^{238}Pu]_{in}$ 6.0–7.6·10^{-12} M. Distribution ratios (onwards denoted as R_d) reported by the authors largely varied (from 10^3 to $7 \cdot 10^4$ dm^3 kg^{-1} on NRVB) depending on the phase separation method used (filter pore size from 5 µm to 30′000 Da MWCO). Aggarwal et al. studied the uptake of Pu(IV) by ordinary Portland cement blends and C–S–H phases in the pH-range of 12.2–12.6 (Aggarwal et al., 2000). The authors obtained similarly high R_d values for cement and C–S–H phases (≈3·10^5 dm^3 kg^{-1}), and concluded that the latter phases are the main sink for Pu in hardened cement paste (HCP). Pointeau and co-workers conducted a comprehensive study on the uptake of Pu(IV) by two cements (CEM I and CEM V) in different degradation stages, as well as with C–S–H phases with different Ca:Si ratios (Pointeau et al., 2004). Experiments were performed with [238]Pu, hydrazine as redox buffer, S:L 0.5 g dm^{-3} and ultracentrifugation (1 h at 50000 g) as phase separation. The authors reported R_d values ranging between 10^4 and 10^6 dm^3 kg^{-1}, witnessing higher values for C–S–H phases.

Pu(IV) and Np(IV) have similar ionic radii, i.e. 1.01 and 1.02 Å, respectively (Neck and Kim, 2001), and thus are often considered as close chemical analogues in terms of aqueous speciation and sorption properties. Tits and co-workers performed a comprehensive study on the uptake of [239]Np(IV,V,VI) by C–S–H phases of different Ca:Si ratios (Tits et al., 2014b). Experiments with Np(IV) in the presence of $Na_2S_2O_4$ after phase separation by ultracentrifugation (1 h at 90000 g) yielded a strong uptake ($R_d \approx 3 \cdot 10^5$ to ≈3·10^6 dm^3 kg^{-1}), independently of the pH and Ca:Si ratio.

Two recent review works have critically reexamined the available data for the uptake of Pu by cement in the degradation stages I to III (Ochs et al., 2016; Wieland, 2014). Based on the available literature but mostly relying on extensive datasets reported for Th(IV) and Np(IV), Wieland selected the same R_d value (10^5 dm^3 kg^{-1}) for all An(IV) and all degradation stages of cement (Wieland, 2014). In contrast to this selection, Ochs and co-workers proposed a lower R_d value ($5 \cdot 10^3$ dm^3 kg^{-1}) for the degradation stage I of cement, followed by slightly higher R_d value ($3 \cdot 10^4$ dm^3 kg^{-1}) for degradation stages II and III, based on pessimistic assumptions.

Isosaccharinic acid, a polyhydroxy carboxylic acid ($C_6H_{12}O_6$, HISA), is the main degradation product of cellulose in the Ca-rich hyperalkaline solutions defined by cementitious systems (Glaus and Van Loon, 2008; Glaus et al., 1999). In alkaline solutions, the ligand exists mainly in the carboxylate form (as ISA$^-$ ions or denoted simply as ISA), nevertheless at higher alkalinity of the media (Evans, 2003) or in a metal-ligand complex species, it may lose one or more of the hydroxyl group proton(s), forming a double or higher negatively charged ion written as $ISA_{-xH}^{-(1+x)}$. The free concentration of ISA in the pore water of cementitious systems is strongly defined by the initial cellulose inventory and the sorption of the ISA ligand onto cement phases. The latter strongly depends upon a number of parameters such as pH, [Ca], S:L or average surface charge or coverage (Pointeau et al., 2006a, 2006b, 2008; Van Loon and Glaus, 1998; Van Loon et al., 1997).

ISA has been shown to form strong complexes with An(III)/Ln(III) and An(IV) under hyperalkaline conditions (Gaona et al., 2008; Moreton, 1993; Moreton et al., 2000; Rai et al., 2003; Rai and Kitamura, 2017; Tasi et al., 2018a, b; Tits et al., 2005; Vercammen et al., 2001). The presence of high concentrations of Ca as expected during degradation stage II of cement ([Ca] ≈ 0.02 M) further promotes the formation of stable quaternary complexes Ca(II)–An(IV)–OH–ISA (Tasi et al., 2018b; Tits et al., 2005; Vercammen et al., 2001). Such complexes can substantially decrease the uptake of radionuclides by cement and thus enhance their mobility in underground repositories.

In experimental studies investigating the uptake of strongly sorbing radionuclides in the presence of complexing ligands, two main constraints have to be considered: (i) the lowest radionuclide concentration that can be quantified for the given experimental conditions (or the maximum value for the sorption distribution ratio), and (ii) the stability of the cementitious material at increasing ligand concentrations. Literature data on the uptake of An(IV) by cement in the presence of ISA system are based on studies dealing with Th(IV) (Holgersson et al., 1998; Wieland et al., 2002). Some of these studies were performed with very low S:L (0.1 g·dm^{-3}), and thus fall outside the stability field of HCP at ligand concentrations above ≈ 10$^{-3.5}$ M (as discussed elsewhere (Wieland, 2014)). Experiments with higher S:L (≥1 g·dm^{-3}) generally resulted in a decrease in R_d values at ISA concentrations above ≈ 10^{-4} M.

The only two experimental studies in this context focusing on Pu and ISA provide limited insights on its uptake by cement in the presence of ISA (Baston et al., 1995; Greenfield et al., 1997). Experimental details of the sorption study by Baston and co-workers in the absence of ISA were summarized above. Under analogous boundary conditions, the authors investigated the uptake of Pu at pH 12.4 in the presence of [ISA] 2·10^{-3} M. At this ligand concentration, the reported R_d values ranged between 68 and 190 dm^3·kg^{-1} (depending upon phase separation method). This represents a significant decrease in the distribution coefficients compared to the ISA-free systems (R_d 1.4–6.4·10^6 dm^3 kg^{-1}). The effect was attributed to the formation of the aqueous complex $Pu(V)O_2ISA_{-2H}^{2-}$, which is a speculative assumption as previously discussed.

Greenfield and co-workers investigated the effect of the degradation products of cellulose on the solubility and sorption (onto NRVB) of selected radionuclides (Greenfield et al., 1997). Experiments were performed under N_2-atmosphere, with S:L 50 g dm^{-3}, pH (12.0 ± 0.1) and using cellulose degradation leachates generated under anoxic conditions with ISA at a constant ligand concentration of 10^{-2} M. Plutonium was introduced into the system as [238]Pu(IV), and no redox buffer was applied. In the presence of ISA, the authors reported an R_d value of 2·10^2 dm^3 kg^{-1}, compared to R_d 5·10^4 dm^3 kg^{-1} in the absence of ISA. Although the experimental conditions in Baston et al. (1995) and Greenfield et al. (1997) are remarkably different, it is worth noting that the higher ISA concentration used in Greenfield et al. (1997) apparently resulted in a weaker impact on the uptake process compared to the findings of Baston et al. (1995).

Thorium is often considered as a "redox-insensitive" substitute for An (IV) (with An U, Np, Pu), and for this reason, it has been extensively used to investigate complexation reactions and sorption processes under repository-relevant conditions. The use of Th(IV) however, does not capture the specific impact that the redox conditions may have on

complexation or sorption processes. Furthermore, Th(IV) has the largest radius among the tetravalent actinides ions ($r_{Th^{4+}}$ 1.08 Å, $r_{U^{4+}}$ 1.04 Å, $r_{Np^{4+}}$ 1.02 Å, $r_{Pu^{4+}}$ 1.01 Å) (Neck and Kim, 2001), which was shown to significantly impact its solution chemistry. For instance, Th(IV) exhibits much weaker hydrolysis than Pu(IV) (Th: log $*\beta°_{(1,1)}$ –(2.5 ± 0.5); Pu: log $*\beta°_{(1,1)}$ –(0.54 ± 0.06)) (Guillaumont et al., 2003; Rand et al., 2009). More specifically, we have recently shown that the aqueous complexes forming in the system Ca(II)–Pu(IV)–ISA (Tasi et al., 2018a,b) clearly differ from those reported for the system Ca(II)–Th (IV)–ISA (Tits et al., 2005; Vercammen et al., 2001).

Hence, there is a clear need to quantify the processes responsible for the uptake of Pu in cementitious environments. The present study aims at a comprehensive investigation of Pu uptake by cement in the presence of ISA under reducing conditions. The work focusses on cement type CEM I at degradation stage II, which is considered as the most relevant degradation stage of cement in the context of L/ILW due to its long residence time expected under repository conditions. Experiments are performed under well-defined redox conditions, which feed into the interpretation of the oxidation state distribution of Pu under conditions of interest. Specific efforts are dedicated to understand the sorption of ISA and its impact on the surface chemistry of cement, as a pre-requisite to properly understanding the ternary system cement–Pu–ISA. This work builds on our previous studies on the redox chemistry of Pu in alkaline to hyperalkaline systems (Tasi et al., 2018c), and on the solution chemistry and thermodynamics of the system Pu(III/IV)–ISA in the absence (Tasi et al., 2018a) and presence of Ca (Tasi et al., 2018b).

2. Experimental

Experiments involving the use of plutonium were performed in specialized α-laboratories within the controlled area of KIT–INE. All experiments were conducted in gloveboxes at T (22 ± 2) °C under Ar-atmosphere with O_2 concentration below 2 ppm, except otherwise indicated.

2.1. Chemicals

Aqueous solutions were prepared using ultra–pure water from a Milli–Q apparatus (Millipore, 18.2 MΩ, 22 ± 2 °C) and purged for several hours with Ar before use. The Milli–Q water used for the preparation of ISA-containing solutions was further boiled for several hours with the simultaneous purge of Ar. Diethyl–ether ($C_4H_{10}O$, p.a.), NaCl (p.a.), NaOH (Titrisol), KOH (p.a.), HCl (Titrisol), $Na_2S_2O_4$ (>87%), hydroquinone (p.a.), Propan-2-ol (>99.9%, for spectroscopy ®Uvasol) were obtained from Merck. $SnCl_2$ (p.a.) was purchased from Sigma-–Aldrich. Carbonate impurities in fresh 1.0 M NaOH (Titrisol) were quantified as $(3 ± 1) \cdot 10^{-5}$ M using a Shimadzu TOC-L equipment (Shimadzu, Kyoto, Japan, for quantification details see section 2.4.1). Ca $(ISA)_2(s)$ [$CaC_{12}H_{22}O_{12}$] was purchased from Alfa Aesar. NaISA(s) was prepared by an ion exchange method from commercial Ca(ISA)$_2$(s) using an ion exchange resin (Chelex® 100, Na-form, Sigma Aldrich, analytical grade purity) and diethyl–ether ($C_4H_{10}O$, ACS reagent grade, VWR BDH Prolabo®). A detailed description of the synthesis, purification and characterization of NaISA(s) is provided elsewhere (Tasi et al., 2018a). The final stock solution resulted in (0.16 ± 0.02) M NaISA at pH_c 8.9, with an excess of 0.18 M NaCl.

The isotopic composition of the Pu used in this study was 99.4 wt % ^{242}Pu, 0.58 wt % ^{239}Pu, 0.005 wt % ^{238}Pu and 0.005 wt % ^{241}Pu as characterized via inductively couple plasma quadrupole mass spectrometry (ICP-MS). In solubility experiments, the use of the long-lived ^{242}Pu isotope ($t_{1/2}$ $3.75 \cdot 10^5$ a) significantly reduces the occurrence of redox processes induced by radiolysis.

Plutonium was spiked to most of the samples (except in the "solubility experiments", see Section 2.4.3.1) as Pu(VI), to avoid large oversaturation conditions with respect to the sparingly soluble PuO_2(am, hyd) (see Tasi et al., 2018a). Under the redox conditions of the present study controlled by hydroquinone, $Na_2S_2O_4$ and Sn(II), higher oxidation states of Pu (+V, +VI) are expected to be reduced within few hours to minutes to the +IV or + III state (Fellhauer, 2013). The Pu(VI) stock solution was prepared by dissolving a radiochemically pure Na_2^{242}Pu $(VI)_2O_7 \cdot x H_2O$(cr) solid phase previously prepared in our laboratory (Schepperle, 2020). The resulting stock solution was characterized by UV–Vis–NIR spectroscopy, and the total Pu concentration was accurately quantified by a combination of liquid scintillation counting (LSC), standard ICP-MS and sector field inductively coupled plasma mass spectrometry (SF-ICP-MS) techniques. Additional details on the preparation and characterization of the Pu(VI) stock solution are provided as Supplementary Information (Section SI-1.1).

Hydrated cement rods were obtained from the Swedish Nuclear Fuel and Waste Management Company (SKB). The specimens were cast from a mixture of Swedish structural Portland cement for civil engineering (CEM I 42.5N BV/SR/LA) and deionized water at a water-to-cement weight ratio of 0.5. The chemical composition of the non-hydrated cement as provided by the manufacturer is included in the Supplementary Information (Section SI-1.2).

2.2. Measurements of pH and E_h

The total free concentration of protons, in molar (M, in mol·dm^{-3}) units (pH_c –log ([H$^+$]/M)) was determined using combination pH–electrodes (type Orion Ross, Thermo Scientific) freshly calibrated against standard pH buffers (pH 3–13, Merck). In aqueous solutions of ionic strength $I \geq 0.1$ M, the measured pH value (pH_{exp}) is an operational, apparent value related to [H$^+$] by pH_c $pH_{exp} + A_c$, where A_c is an empirical parameter for a given background electrolyte, ionic strength and temperature. Correction of the measured pH_{exp} values in the investigated pore water solutions (with ionic strength of $I \sim 0.1$ M) considered Ca^{2+} ion as main constituent. Empirical A_c values for CaCl$_2$ systems were adapted from the literature (Altmaier et al., 2008). Due to the high hydroxide concentration ([OH$^-$] ≈ 0.03 M) and the presence of varying ISA total concentrations (6 ≤ log ([ISA]$_{tot}$/M) ≤ 2) that may alter the equilibrium of the Ca-system, total H$^+$ concentrations were also calculated for comparative purposes. The calculation of [H$^+$] was based on the experimentally measured [Ca]$_{tot}$, [ISA]$_{tot}$ and assumed the saturation with respect to portlandite. Thermodynamic data for the system Ca(II)-HISA-OH were taken from the NEA–TDB review book by Hummel and co-workers (Hummel et al., 2005). In all cases, the agreement between experimental and calculated pH_c was satisfactory (considering associated uncertainties: ± 0.05 pH units).

The redox potential in solution was determined with combined Pt or Au and Ag/AgCl reference electrodes (Metrohm). Measured potentials were converted to E_h (versus standard hydrogen electrode, SHE) by correcting for the potential of the Ag/AgCl inner-reference electrode at 3 M KCl and T 22 °C (+207 mV). E_h values were converted to pe –log a_e^- according to the following equation:

$$E_h \quad -RT \ln(10) \, F^{-1} \log a_e^-, \tag{1}$$

where R is the ideal gas constant (8.31446 J mol^{-1} K^{-1}), F is the Faraday constant (96485.33 C mol^{-1}) and a_e^- is the activity of the electron in solution. E_h values of the solutions were collected following the approach described in our previous studies (Tasi et al., 2018a, 2018c). The uncertainty of the measured E_h values (calculated as 2σ of repeated measurements) ranged between ± 15 and ± 30 mV.

2.3. Initial cement powder and cement pore water

The cement paste rods were first ground with manual crushing, followed by milling with an agate-ball (m 0.50 kg, diameter of 70 mm) mill (®pulverisette 0, Fritsch GmbH) under ambient conditions. The sieving of the ground material involved a continuous-flow, vibrational sieving mill (®pulverisette 0, Fritsch GmbH) equipped with stainless

steel sieves. The resulting powder with particle diameter size $<100\,\mu m$ was characterized by X-ray powder diffraction (XRD), X-ray photoelectron spectroscopy (XPS) and thermogravimetric analysis coupled with differential scanning calorimetry (TG–DSC). After digestion with $6.0\,M\,HNO_3$, the elemental composition of cement was further characterized using ICP-MS and inductively coupled plasma–optical emission spectroscopy (ICP–OES). Experimental details on the application of specific techniques are provided as Supplementary Information (Section SI-1.3). The well-characterized powder material (hereafter denoted as *initial cement powder*) was used for the preparation of the pore water leachate and in all sorption experiments.

A pore water solution representative of cement degradation stage II was prepared by washing out the alkali content of the cement material. A fraction of the initial cement powder was mixed with $1.8\,dm^{-3}$ of Milli-Q water to attain S:L $\approx 25\,g\cdot dm^{-3}$. The supernatant solution was regularly characterized for 30 days. For this purpose, the pH as well as concentrations of major (Na, K, Ca, Mg) and minor (Al, Ti, V, Cr, Mn, Fe, Co, Ni, Cu, Rb, Ba, Pt) elements were quantified by ICP-OES and ICP-MS after centrifugation ($4020\,g$, 15 min). Equilibrium conditions, *i.e.* constant pH and concentration of major elements within measured uncertainties, were reached in 1 week of contact time.

The initial leachate with high alkali content was separated from the HCP by sedimentation, and replaced by 1.8 L of fresh Milli-Q water to obtain a large volume of pore water solution representative of the cement degradation stage II. This pore water was regularly characterized (pH, concentrations of major and minor elements, non-purgeable organic content (NPOC) and total inorganic content) until attaining equilibrium conditions (after ~2 weeks of contact time). The suspension was kept under Ar atmosphere and used during the complete sorption study as a source of pore water (The composition of the pore water is provided in Section 3.1).

A small quantity (~0.1 g) of the cement phase in equilibrium with the pore water was taken in a suspension and separated by centrifugation (at $4020\,g$ for 15 min) after ~10 months of contact time. Hydration stoppage was achieved with propan-2-ol, and the dried cement powder was characterized by means of XRD, XPS and TG-DSC (see Section SI-1.3 in the Supplementary Information).

2.4. Preparation of batch experiments

All batch samples for sorption- and solubility studies were prepared using the pore water (after centrifugation at $4020\,g$, 15 min) representative of cement degradation stage II (see Section 3.1 for the composition). This pore water was used in combination with the initial dry cement powder for the preparation of batch sorption experiments with known S:L.

Section 2.4.1 summarizes the experimental procedure for the binary system cement-ISA. This set of experiments includes the quantification of the ISA uptake by cement, and characterization of the impact of ISA on zeta potentials of suspended cement particles. Sorption experiments in the binary system cement–Pu described in Section 2.4.2 aimed at providing a "sorption baseline" in the interpretation of the Pu uptake in the presence of ISA. The ternary system cement–Pu–ISA was investigated using three different approaches: (i) sorption experiments at varying S:L and ISA concentrations (Section 2.4.3.2); (ii) desorption experiments (Section 2.4.3.3); and (iii) sorption experiments coupled to solubility experiments with PuO_2(ncr,hyd) (Section 2.4.3.4). A series of solubility experiments with PuO_2(ncr,hyd) using cement pore water with varying concentrations of ISA (Section 2.4.3.1) was performed to evaluate upper solubility limits under the specific conditions of the sorption experiments, but also to provide supernatant solutions for the sorption experiments in (iii). Applied total concentration ranges considered for ISA was based upon preliminary thermodynamic calculations avoiding the precipitation of the $Ca(ISA)_2$(s) phase.

2.4.1. Cement–ISA system

The uptake of ISA by the HCP was investigated in two series of independent batch experiments ($V_{liquid} \approx 10\,cm^3$, 11 batches in total): (i) S:L constant $\approx 4\,g\cdot dm^{-3}$, log ($[ISA]_{tot}/M$) $\approx$ 5, 4, 3, 2; and (ii) log ($[ISA]_{tot}/M$) constant $\approx 3\,M$, S:L $\approx$ 2, 4, 8, 15, 20 and 50 g·dm^{-3}. In order to assess the organic carbon content leaching from the HCP (due to the presence of organic additives in the original material), a third series of experiments with S:L $\approx$ 2, 4, 8, 15, 20 and 50 g·dm^{-3} was prepared in the absence of the ligand. The latter experiments served as the basis for background correction of the sorption data on the cement-ISA system.

The pH was systematically monitored for all samples. After 7 and 14 days of contact time, aliquots of the supernatant solutions containing ISA were centrifuged at $4020\,g$ for 15 min, transferred (20–500 μdm^3, depending upon ISA concentration) into 2 w% HNO_3 solutions and analyzed for NPOC using a Shimadzu TOC-L instrument (Shimadzu, Kyoto, Japan). The internal furnace of the equipment is filled with preconditioned platinum impregnated high sensitivity catalyst operating at $680\,°C$. Prior to analyses via a nondispersive infrared sensor, combustion products are carried by high purity O_2 gas-flow through a 25% H_3PO_4 solution, a dehumidifier, a halogen scrubber and a particle filter for the removal of disturbing impurities. Considering the detection limit of the technique (≈ 0.1 ppm) and the organic impurities/additives present in cement, the lowest quantifiable ISA concentration was $\approx 2.5\cdot10^{-5}\,M$.

The possible impact of ISA on the dissolution of portlandite was specifically investigated for a sample with S:L $\approx 2\,g\cdot dm^{-3}$ and log ($[ISA]_{tot}/M$) ≈ 2. After a contact time of 14 days, the supernatant solution was characterized with respect to pH, major (Na, K, Ca, Mg) and minor (Al, Ti, V, Cr, Mn, Fe, Co, Ni, Cu, Rb, Ba, Pt) metal ion concentrations by ICP-OES and ICP-MS techniques. The resulting solid phase was separated by centrifugation ($4020\,g$, 15 min) and characterized by XRD, XPS and TG-DSC techniques (see Section 2.6) after stopping hydration with propan-2-ol.

The impact of ISA on the electrophoretic mobility of the suspended HCP colloidal particles was investigated in a series of independent batch experiments ($V_{liquid} \approx 10\,cm^3$, 10 batches in total) with S:L $\approx 4\,g\cdot dm^{-3}$ and log ($[ISA]_{tot}/M$) $\approx$ 6, 5.5, 5, 4.5, 4, 3.5, 3, 2.5 and 2. Selected samples were prepared in duplicates to account for the uncertainty of the overall process. One additional batch without ISA was also prepared to test the reproducibility of reported literature values for suspended CEM I type HCP particles under the conditions of interest. After 14 days of contact time, aliquots of the manually suspended particles were transferred into a pre-washed and dried plastic cuvette equipped with the measurement cell and sealed under Ar atmosphere with parafilm. Electrophoretic mobility measurements were performed with a Nanobrook 90 plus PALS (Brookhaven Instruments Co.) equipment. Electropheretic mobilities were recalculated to zeta potentials (ζ) with the built-in software using the Smoluchovsky equation. Fifteen ζ potential values were acquired and averaged for each data point, whereas 15 points were collected for each sample and in the course of one measurement. Each sample was measured twice: in a freshly agitated state and after 15 min of waiting time to account for settling effects. The uncertainty related to the acquisition of a single data point, *i.e.* collection of 15 ζ potential values, was $\pm0.20\,mV$. For one measurement, equivalent to the acquisition of 225 values, the uncertainty was found to be $\pm4\,mV$. For a single ISA total concentration, the maximum detected uncertainty was $\pm9\,mV$ (for log ($[ISA]_{tot}/M$) ≈ 3.5), calculated as 3 times the standard deviation of all data points collected.

All experiments conducted for the binary system cement-ISA are summarized in Table 1.

2.4.2. Cement–Pu system

A total of 23 batch samples were prepared for the characterization of the binary system cement-Pu ($V_{tot} \approx 10\,cm^3$) under absence of ISA. In the course of these experiments, a specified amount of cement powder was contacted with pore water solutions containing a reducing agent

Table 1

Summary of the experiments performed for the binary system cement–ISA.

Experiment description	S:L [g·dm^{-3}]	log ([ISA]$_{tot}$/M)	Measurements
Organic content in cement (additives)	2, 4, 8, 15, 20, 50	–	pH, NPOC
Uptake of ISA; constant [ISA]$_{tot}$	2, 4, 8, 15, 20, 50	−3	pH, NPOC
Uptake of ISA; Constant S:L	4	−5, −4, −3, −2	pH, NPOC
Impact of ISA on portlandite/ cement stability	2	−2	Aqueous phase: pH, concentration of major and minor metal ions; Solid phase: XRD, XPS, TG-DSC
Characterization of zeta potential	4	−6, −5.5, −5, −4.5, −4, −3.5, −3, −2.5, −2	Electrophoretic mobility via PALS

(2 mM HQ, Sn(II) or S$_2$O$_4^{2-}$) targeting S:L of ≈0.1 g·dm^{-3} – 4 g·dm^{-3}. The resulting suspensions were equilibrated for 2 days before the addition of Pu. Negligible volumes (10–20 μdm^{-3}) of the diluted Pu(VI) stock solution were introduced to these systems aiming at initial total Pu concentration of log ([Pu]$_{in}$/M) ≈ −6 or −9. After a first centrifugation step (using a standard lab centrifuge, 4020 g, 15 min), values of pH$_c$, E_h and [Pu]$_{aq}$ were monitored in the supernatant solutions up to $t \leq 4$ months. Phase separation was achieved in the following by ultrafiltration (10 kDa MWCO, average pore diameter size ≈ 2–3 nm) or ultracentrifugation (Beckman XL-90, rotor type 90Ti, 694000 g, 1 h). Additional details on the sampling procedure are provided in Section 2.5. A summary of all experiments conducted for the binary system cement–Pu is provided in Table 2.

To assess the oxidation state of plutonium in the binary system cement-Pu and to evaluate the possible precipitation of Pu in the most concentrated systems, the solid phase of selected sorption samples (S:L ≈ 2 g·dm^{-3}, log ([Pu]$_{in}$/M) ≈ −6, t_{eq} ≈ 132 d, reducing system: Sn(II) and HQ) were retrieved after centrifugation (4020 g, 15 min) and characterized *in-situ* by Pu L$_{III}$-edge XANES measurements (at INE–Beamline, see Section 2.6 for more information). The sample equilibrated in HQ was also characterized *ex-situ* by XPS (see Supplementary Information, SI-1.3 and Section 2.6).

A number of cement samples contacted with Pu for t ≈ 167 d were separated from the supernatant solution (centrifugation at 4020 g, 15 min) and used in a series of desorption experiments in the presence of ISA. Details on the preparation of these batch experiments are provided in Section 2.4.3.3.

2.4.3. Cement–Pu–ISA system

2.4.3.1. Solubility experiments with PuO$_2$(ncr,hyd) in cement pore water systems.
Samples were prepared by introducing 0.2–1 mg of a well-characterized PuO$_2$(ncr,hyd) solid phase (Tasi et al., 2018c) in cement pore water solutions pre-equilibrated with 2 mM HQ and log ([ISA]$_{tot}$/M) = −5 (1), −4 (1), −3 (8) and −2 (1) (in brackets: total number of batches; V$_{tot}$ ≈ 25 cm^3 per batch sample). The values of pH$_c$, E_h and [Pu] were monitored for 90 days. Equilibrium conditions were attained at $t \approx 30$ days. After terminating the solubility experiments, the supernatant solutions were separated by centrifugation at 4020 g for 30 min, and further used in the sorption experiments described in Section 2.4.3.4.

2.4.3.2. Sorption experiments with varying S:L and ISA total concentrations.
Batch experiments on the ternary system cement–Pu–ISA were conducted for $0.2 \leq$ S:L/g·dm$^3 \leq 50$ and $−6 \leq$ log ([ISA]$_{tot}$/M) $\leq −2$, with V$_{tot}$ = 5 or 10 cm^3. Experiments were performed in the presence of reducing buffers, *i.e.* HQ, Sn(II) or Na$_2$S$_2$O$_4$. The impact of the order of addition of the individual components (cement/Pu/ISA) on the overall uptake was specifically investigated in two experimental series: (i) *(Pu + cement) + ISA* and (ii) *(Pu + ISA) + cement*. In option (i), the cement powder was contacted for 2 days with a pore water solution containing Pu and the chosen redox buffer, before ISA was added to the system. In case of option (ii), Pu and ISA were equilibrated for 2 days in the pore water solution containing the given redox buffer, and then a certain amount of cement powder was added to the solution to obtain the targeted S:L. Details on the different experimental series are summarized in Table 2.

After the addition of the last component, values of pH$_c$, E_h and [Pu] (after solid phase separation via centrifugation, ultrafiltration or ultracentrifugation) were regularly monitored for 4 months. Details on the quantification of Pu total concentrations in the aqueous phases are provided in Section 2.5.

The redox state of Pu in selected samples (S:L ≈ 2 g·dm^{-3}, log ([Pu]$_{in}$/M) ≈ −6, t ≈ 130 d, redox buffer Sn(II) or HQ) was investigated by XAFS and XPS techniques. For this purpose the cement pastes were compacted by centrifugation (4020 g, 15 min) and analyzed *in-situ* by Pu L$_{III}$-edge XANES. An aliquot of the sample equilibrated in HQ was also characterized *ex-situ* by XPS. A detailed description of these instrumental techniques is provided in Section 2.6.

2.4.3.3. Desorption experiments.
Desorption experiments were performed using solid phases retrieved from selected sorption samples of the binary system cement–Pu. The original samples (6 individual batches) were equilibrated for t ≈ 167 days with S:L ≈ 0.2–2.5 g·dm^{-3} and log ([Pu]$_{in}$/M) ≈ −9 (see Section 2.4.2). The cement paste was

Table 2

Summary of the experiments performed for the binary and ternary systems cement–Pu and cement–Pu–ISA, respectively.

Experiment Description	Number of batches	S:L/ g·dm^{-3}	log ([ISA]$_{tot}$/ M)	log ([Pu]$_{in}$/M)	Redox buffer	Order of addition
Sorption (binary)	23	0.2–50	–	−6, −9	HQ, Sn(II), S$_2$O$_4^{2-}$	–
Solubility	11	–	−5, −4, −3, −2	equilibrium with PuO$_2$(ncr, hyd)[a]	HQ	–
Sorption (ternary)	24	0.2	−3, −2	−6, −9	HQ, Sn(II), S$_2$O$_4^{2-}$	(Pu + cement) + ISA (Pu + ISA) + cement
	12	2	−3, −2	−6, −9	HQ, S$_2$O$_4^{2-}$	(Pu + cement) + ISA (Pu + ISA) + cement
	9	2	−6 to −2	−9	HQ	(Pu + cement) + ISA
Desorption (ternary)	6	0.2–2.5	−3, −2	−9	HQ	analogous to (Pu + cement) + ISA
Sorption (ternary). Supernatant from solubility Experiments	9	0.2–50	−3	equilibrium with PuO$_2$(ncr, hyd)	HQ	analogous to (Pu + ISA) + cement

[a] Ncr refers to the nanocrystalline character of the solid phase, see (Tasi et al., 2018c).

separated from the supernatant by centrifugation (4020 g, 15 min), and immediately contacted with a new pore water solution containing 2 mM HQ and log ([ISA]$_{tot}$/M) ≈ 3 or ≈ 2. The S:L of the original sample was retained. A summary of the experimental conditions considered for these experiments is provided in Table 2. The values of pH$_c$, E$_h$ and [Pu]$_{aq}$ were monitored after solid phase separation (via centrifugation and ultrafiltration) for $t \leq 4$ months (see Section 2.5 for more details).

2.4.3.4. Sorption experiments coupled with undersaturation solubility experiments. The supernatant solutions collected from the solubility experiments with PuO$_2$(ncr,hyd) in the presence of ISA after an equilibration time of 54 days (see Section 2.4.3.1) were considered for the preparation of a new series of sorption experiments. This approach avoids oversaturation conditions in the sorption experiments, whilst maximizing the initial Pu concentration introduced.

Supernatant solutions in equilibrium with PuO$_2$(ncr,hyd) containing Pu (log ([Pu]$_{in}$/M) ≈ 8.5 ± 0.5) and ISA (with log ([ISA]$_{tot}$/M) ≈ 3) were separated from the solid phase by centrifugation at 4020 g (15 min). These solutions with volumes of 10 cm^3 were added to certain amounts of the initial cement powder to achieve S:L ≈ 0.2–50 g·dm^{-3} (see Table 3). Consequently, this new series of sorption samples follows an analogous sequence as the sorption experiments *(Pu + ISA) + cement* described in Section 2.4.3.2. Values of pH$_c$, E$_h$ and [Pu]$_{aq}$ were monitored after solid phase separation (via centrifugation and ultrafiltration) for $t \leq 14$ months (see Section 2.5 for more details).

2.5. Characterization of the aqueous phase

The quantification of total Pu concentrations in the aqueous phase were performed after phase separations. In a first step, samples were centrifuged at 4020 g for 15 min to deposit any suspended particles. Subsequently, aliquots of 250–350 µdm^{-3} were taken from the clear supernatant and either acidified with 2% HNO$_3$ solution or transferred to a 10 kDa filter (pore diameter size ≈ 2–3 nm, Nanosep ®, Pall Life Sciences), centrifuged at 4020 g for 15 min and the filtrate was then acidified with 2% HNO$_3$. The first aliquot aimed at the quantification of total Pu concentration including intrinsic Pu(IV) colloids, whereas the ultrafiltered solution provided information on the total amount of dissolved Pu concentration. For selected samples, phase separation was also performed by ultracentrifugation (Beckman XL-90, rotor type 90Ti). In this case, a larger volume of the supernatant solution (3–4 cm^3) was centrifuged at 694000 g in welded vials for one hour, after which a known volume of the supernatant was acidified with 2% HNO$_3$. In all cases, the acidic solutions were analysed for the aqueous total concentration of Pu either by standard ICP–MS, SF–ICP–MS or via liquid scintillation counting (LSC) using the signal of the low-energetic β-emitter ^{241}Pu. For the latter case, aliquots of the acidified supernatant were mixed with 10 cm^3 of LSC cocktail (Ultima Gold XR, Perkin Elmer) and measured on a low-level LSC equipment type Quantulus 1220 (LKB WallacOy, Turku, Finland, PerkinElmer) for 30 min. Standard addition with 50 µdm^3 of a well-defined Pu stock solution (4.36·10^{-7} M or 3.18·10^{-7} M) with the same isotopic composition was used to overcome

the matrix solution effect on the counting efficiency of ^{241}Pu of the unknown samples. The detection limits (DL) for Pu under conditions of the present study are ~10$^{-10.5}$ M (ICP–MS), ~10^{-13} M (SF–ICP–MS) and ~10^{-9} M (LSC).

All plutonium concentrations quantified by either LSC or (SF–) ICP–MS are reported in molar units (M, in mol·dm^{-3}). Total aqueous Pu concentrations determined in the course of sorption experiments are denoted as [Pu]$_{aq}$, whereas Pu concentrations in the solubility experiments are referred to as [Pu]$_{tot}$. Note, that just as observed in our former study (Tasi et al., 2018b), Pu concentrations quantified after ultracentrifugation and ultrafiltration or directly in the supernatant solutions (after centrifugation) were practically identical in all ISA-containing experiments of the present study. This observation confirms the important role of Ca(II) in the destabilization of "Pu(IV)–ISA colloids" (Tasi et al., 2018b).

In order to maintain constant S:L throughout the complete experiment, each sample was refilled to the same original volume after each sampling step. A Pu-free matrix solution of identical composition was used for this purpose. The impact of this procedure on the total molar amount of Pu in the system was calculated to be negligible (Δ ~ 3–0.1%).

2.6. Characterization of the solid phase

The initial cement powder and the cement solid phases equilibrated with the cement pore water (in the absence and presence of Pu) were characterized with the techniques summarized below (XPS and XANES). More XRD, XPS and TG-DSC analyses are described in the Supplementary Information (SI-1.3). For selected samples in the absence of Pu, the solid cement phases (with m$_{cement}$ ≈ 0.08–0.5 g) were treated with propan-2-ol (20 cm^3) to stop the hydration process (Scrivener et al., 2016). For this purpose, the cement paste retrieved after a centrifugation step at 4020 g (15 min) was immersed in the organic phase for 20 min. The suspension was then filtered through a PTFE membrane with 5 µm pore size (Millipore) using a vacuum pump (Becker). The resulting paste was dried in an oven for 20 min at 40 °C and stored in sealed vials under Ar atmosphere until characterization.

2.6.1. X-ray photoelectron spectroscopy

Selected cement samples were characterized by XPS to assess surface elemental composition and (for the sample containing Pu) oxidation state analysis. The samples were prepared on an indium foil and mounted on a sample holder under anoxic conditions (Ar atmosphere). XPS measurements were performed using a PHI 5000 VersaProbe II (ULVAC-PHI Inc.) system equipped with a scanning microprobe X-ray source (monochromatic Al Kα (1486.7 eV) X-rays) in combination with an electron flood gun and a floating ion gun generating low energy electrons (1 eV) and low energy argon ions (6 eV) for charge compensation at isolating samples (dual beam technique), respectively. Survey scans were recorded with an X-ray source power of 31 W and pass energy of 187.85 eV. Narrow scans of the elemental lines were recorded at 23.5 eV pass energy of the analyser which yields an energy resolution of

Table 3

pH$_c$ and concentrations of relevant metal ions as quantified by ICP-OES/MS techniques of the liquid phases in contact with different cement pastes. The "Cement pore water" designates the solution generated by equilibrating Milli-Q water with the pre-washed cement powder (t = 1 a). The "ISA-cement pore water" corresponds to the supernatant of the sample prepared using the "pore water" with log ([ISA]$_{tot}$/M) = 2 at S:L = 2 g·dm^{-3}, after a contact time of t = 14 d.

Sample name	pH$_c$	Ca(II)	Na(I)	K(I)	Al(III)	Si(IV)	Mg(II)	Fe(III)
		[M] *	[M] *	[M] *	[M] **	*[M]**	*[M]**	[M] **
Cement pore water	(12.55 ± 0.08)	0.021	7·10^{-5}	3·10^{-4}	2·10^{-6}	< D.L.^{a}	8·10^{-7}	3·10^{-8}
ISA-cement pore water	(12.60 ± 0.03)	0.021	0.02^b	8·10^{-4}	2·10^{-5}	7·10^{-5}	2·10^{-6}	5·10^{-6}

*Related uncertainties are ± 5–20%.

** Related uncertainties are at least ± 50%.

^{a} Below detection limit, *i.e.* < 1 10^{-5} M for Si(IV).

^{b} The elevated Na-content is caused by the use of a NaISA stock solution.

0.69 eV full width at half maximum (FWHM) on the Ag $3d_{5/2}$ elemental line of pure silver. Calibration of the binding energy scale of the spectrometer was performed using well-established binding energies of elemental lines of pure metals (monochromatic Al K_α: Cu $2p_{3/2}$ at 932.62 eV, Au $4f_{7/2}$ at 83.96 eV) (Seah et al., 1998). C 1s of hydrocarbon at 284.8 eV is used as charge reference. The error in binding energies of elemental lines is estimated to be ± 0.2 eV. Data analysis was performed using ULVAC-PHI MultiPak software, version 9.6.

2.6.2. Pu L_{III}-edge X-ray absorption near-edge spectra (XANES) measurements

The oxidation state of Pu in selected solid phases of the cement–Pu and cement–Pu–ISA systems was characterized by Pu L_{III}-edge XANES at the INE–Beamline for Actinide Research at the Karlsruhe Research Accelerator (KARA), KIT Campus Nord (Rothe et al., 2012). The storage ring was operated at 2.5 GeV electron energy with a mean electron current of 120 mA.

Aliquots of the suspensions containing the cement paste ($\approx$10–20 mg) equilibrated with Pu (in the absence and presence of ISA) were transferred within the glove box into 400 μL polyethylene vials. The vials were tightly sealed with Parafilm (Bemis Company, Inc) and centrifuged at 4020 g for 10 min. The resulting samples were mounted in a gas-tight cell inside the Ar-glovebox and transported to the beamline. During the measurements, Ar was continuously flushed through the cell to ensure inert atmosphere at T (24 ± 2) °C. As the data accumulation on the compacted solid phases was achieved within sealed double containments with separate, protective, inert gas atmosphere and with the original liquid phases also being present on top of the samples, measurement conditions can be considered as *in-situ* in this set up.

The tuneable monochromatic beam was delivered by a double crystal monochromator (DCM), equipped with a pair of Ge(422) crystals (2d 2.3094 Å). Possible higher harmonic radiation was suppressed by detuning the parallel alignment of the crystals to 70%. A piezo-driven feedback system (MOSTAB) allows to stabilize the incident beam intensity to 70% of the rocking curve maximum intensity.

XANES spectra of the Pu L_{III}-edge (E ($2p_{3/2}$) Pu(0): 18,057 eV) were recorded in fluorescence mode using a combination of two Silicon Drift Detectors (SDD)- a Vortex®-ME4 (4 elements) and a Vortex-60EX (1 element) (Hitachi/SIINT, both 1 mm crystal thickness). The incident beam intensity as well as the transmission of the reference Zr metal foil was recorded simultaneously with the fluorescence signal using Ar-filled ionization chambers at ambient pressure. Total of 8–10 scans were collected for each Pu sample. The spectra were calibrated against the first inflection point in the K-edge spectrum of a Zr metal foil (E (1s) Zr (0): 17,998 eV) and averaged to reduce statistical noise. XANES data reduction were performed with the ATHENA software from the Demeter 0.9.026 program package (Ravel and Newville, 2005), following standard procedures for edge jump normalization. The Pu L_{III}-edge XANES spectra obtained in this work were compared with Pu(III) and Pu(IV) reference spectra collected at the INE-Beamline under the same experimental conditions and data analysis procedure (Brendebach et al., 2009; Tasi et al., 2018c; Walther et al., 2009).

2.7. Data evaluation and modelling methods

Equilibrium calculations were performed using the Solver tool of Microsoft Excel and with the PhreePlot – PhreeqC program packages (version 3.3.5, svn 10806) (Kinniburgh and Cooper, 2009; Parkhurst and Appelo, 1999, 2013). The Specific Ion-interaction Theory (SIT) (Ciavatta, 1980) used by NEA–TDB project was adapted for ionic strength corrections. However, due to the low ionic strength in all the experiments ($I \sim 0.10$ M), the main contribution to the activity corrections results from the Debye–Hückel term of the SIT expression.

Thermodynamic data on the Ca^{2+}–Pu^{3+}–Pu^{4+}–OH^-–Cl^-–ISA^-–$H_2O(l)$ system used in work for solubility and speciation calculations of Pu are summarized in Tables A1–A4 in the Appendix.

3. Results and discussion

3.1. Characterization of the pore water solutions in equilibrium with cement paste in the absence and presence of ISA

Solid phase characterization of the cement paste equilibrated with cement pore water in the absence and presence of ISA confirms that the solid phase corresponds to a CEM I type HCP in degradation stage II, and that ISA has a minor impact on the bulk properties of this material (see Supporting Information). The impact of ISA on the surface properties of the cement paste is discussed in Section 3.2.

Table 3 summarizes the pH_c and concentrations of major and minor elements in the pore water equilibrated with the cement (see Section 2.3). The pH_c values and Ca concentrations are in excellent agreement with the values defined via the equilibrium with portlandite, expected for the degradation stage II of cement. The low content of Na and K ($\leq 3 \cdot 10^{-4}$ M) further confirms that the washing of the alkali metal ion content was completed. Note also that the equilibration of the fresh cement powder with the pre-equilibrated pore water also did not result in any deviation from determined properties of the original pore water and the cement powder as described in Table 3 and in the supplementary information (section SI-2.1), respectively.

The impact of ISA on the pore water composition in equilibrium with cement in degradation stage II was evaluated for the highest ISA concentration investigated in this work, *i.e.* log ([ISA]$_{tot}$/M) 2. At this ISA concentration, pH_c and Ca concentration remain mostly unaffected (see Table 3). Calculations using thermodynamic data in Table A-1 of the Appendix predict a slight increase of the Ca concentration in the presence of 0.01 M NaISA (resulting in [Ca(II)]$_{tot}$ 0.0227 M, compared to 0.0204 M in the absence of ISA) due to the formation of the complexes CaISA$^+$ and CaOHISA(aq). The small difference between both values falls within the uncertainty range of the measured Ca concentrations. The remarkable increase in Na concentration in the pore water with ISA originates from the ISA stock solution, which holds a Na: ISA ratio of ≈ 2 (see Section 2.1). This confirms that ISA with log ([ISA]$_{tot}$/M) $\leq$ 2 at S: L ≥ 2 g·dm^{-3} has a relatively low impact on the composition of the cement pore water in degradation stage II.

3.2. Binary system cement–ISA

3.2.1. Uptake of ISA by cement

The uptake of ISA by cement in the degradation stage II was studied at log ([ISA]$_{tot}$/M) constant 3 and S:L 2, 4, 8, 15, 20 and 50 g·dm^{-3}, with t 7 and 14 days. The sorption data shown in Fig. 1 confirm a substantial decrease of ISA concentration in solution with increasing S:L. No significant differences in [ISA]$_{aq}$ were obtained at t 7 and 14 days, suggesting that equilibrium conditions had been attained within this timeframe, consistent with analogous sorption studies, which reported a fast uptake of ISA within 2–3 days (Pointeau et al., 2008; Van Loon and Glaus, 1998; Van Loon et al., 1997).

The observed decrease in ISA concentration reflects rather large distribution ratios, *i.e* log (R$_d$/dm^3·kg^{-1}) ≈ 2.6 in line with ISA sorption data reported by Pointeau et al. (2008) (log (R$_d$/dm^3·kg^{-1}) ≈ 2) under analogous boundary conditions (CEM I, pH 12.5, log ([ISA]$_{tot}$/M) 3.07, presumably at S:L 1 g·dm^{-3}). Discrepancies between datasets can be attributed to differences in the experimental conditions, *e.g.* surface area, S:L used, etc…

Van Loon et al. (1997) studied the uptake of ISA by cement (sulphate resistant, CEM I 55 N HTS) at pH 13.3, $5 \leq$ log ([ISA]$_{tot}$/M) $\leq$ 0.52 and 25 g·dm$^{-3} \leq$ S:L ≤ 500 g·dm^{-3}. The authors observed significant sorption of ISA, which strongly depend on the initial ISA concentration (*e.g.* R$_d \approx 200$ dm^3·kg^{-1} at log ([ISA]$_{tot}$/M) 5, and R$_d \approx 1$ dm^3·kg^{-1} at log ([ISA]$_{tot}$/M) 0.52). The authors empirically simulated their experimental data with a two-site Langmuir-isotherm.

Experimental data either available in the literature or obtained in this work show a strong impact of pH, [ISA]$_{tot}$, [Ca] and S:L on the ISA

uptake by cement. The surface complexation model reported in Pointeau et al. (2008) was validated only at one ISA concentration, and misses the effect of the different sorption sites proposed in Van Loon et al. (1997) in the uptake process. Furthermore, the model of Pointeau and co-workers disregards any variation of the surface properties to model their data within $11.5 \leq pH \leq 13.3$, in spite of the known evolution of the composition of C–S–H phases with varying pH.

The use of a two-site Langmuir-isotherm with the stability constants reported by Van Loon et al. (1997) (orange solid line in Fig. 1) overestimates the $[ISA]_{aq}$ measured under our experimental conditions. This is in line with the observed decrease of ISA sorption at $pH > 12.5$ (Pointeau et al., 2008) and the general trend of anion adsorption with increasing pH.

Considering that all experiments in the present work were performed at $pH_c \approx 12.5$, the fit of experimental data was attempted with a two-site Langmuir-isotherm in the form:

$$[ISA]_{sorbed} = K_1 \cdot q_1 \cdot [ISA]_{aq} \cdot (1 + K_1 \cdot [ISA]_{aq})^{-1} + K_2 \cdot q_2 \cdot [ISA]_{aq} \cdot (1 + K_2 \cdot [ISA]_{aq})^{-1} \qquad (2)$$

To account for the clear correlation between "q" and "K" parameters in Equation (2), the Langmuir-isotherm was fitted by the simultaneous minimization of two separate objective functions (Equations (4) and (5)) derived from Equation (2), i.e. $F_1(q_1, q_2, K_1, K_2)$ and $F_2(q_1, q_2, K_1, K_2)$ using n number of data points.

$$([ISA]_{tot} - [ISA]_{aq}) \cdot V_L \cdot (pore\ water,\ dm^3) \cdot m(cement,\ kg)^{-1}$$

$$[ISA]_{sorbed} = K_1 \cdot q_1 \cdot [ISA]_{aq} \cdot (1 + K_1 \cdot [ISA]_{aq})^{-1} + K_2 \cdot q_2 \cdot [ISA]_{aq} \cdot (1 + K_2 \cdot [ISA]_{aq})^{-1} \qquad (3)$$

$$F_1(q_1, q_2, K_1, K_2) = \left(\sum\nolimits_{i=1}^{n} (\log([ISA]_{sorbed,\ calc.}/M) - \log([ISA]_{sorbed,\ meas.}/M))^2 \cdot (n-1)^{-1} \right)^{0.5} \qquad (4)$$

$$F_2(q_1, q_2, K_1, K_2) = \left(\sum\nolimits_{i=1}^{n} (\log([ISA]_{aq,calc.}/M) - \log([ISA]_{aq,meas.}/M))^2 \cdot (n-1)^{-1} \right)^{0.5} \qquad (5)$$

The modelling approach resulted in the sorption capacities and affinity constants given below in Equation (6), which well explains experimental observations as displayed in Fig. 1 (cyan solid line). In view of the specific adsorption of ISA on calcium-aluminum-silicate-hydrate: C-A-S-H phases (Van Loon and Glaus, 1998), it is important to be mentioned, that derived sorption capacities could be related to the surface site density (of aluminate-type groups) of this solid phase.

$$q_1 = (0.18 \pm 0.02)\ mol \cdot kg^{-1},\ K_1 = (2510 \pm 500)\ dm^3 \cdot mol^{-1}\ and$$

$$q_2 = (0.17 \pm 0.02)\ mol \cdot kg^{-1},\ K_2 = (12 \pm 2)\ dm^3 \cdot mol^{-1} \qquad (6)$$

The cement–ISA sorption model derived in the present study for a two-site Langmuir isotherm at $pH_c \approx 12.5$ is used in the following sections as an empirical formula to calculate $[ISA]_{aq}$ as a function of S:L and $[ISA]_{tot}$.

3.2.2. Impact of ISA on the zeta potentials of suspended HCP particles

Fig. 2 shows the measured ζ potentials of suspended cement particles in the absence and presence of ISA (open and filled symbols, respectively) at various total ligand concentrations. The figure also contains the surface coverage (cyan solid line) of HCP by ISA in percentages as a function of ISA total concentration derived from the Langmuir isotherm using values from Equation (6). Latter calculations considered all experimental conditions, where percentage coverage values were acquired by dividing the normalized, adsorbed ISA concentrations in cement ($mol \cdot g_{cement}^{-1}$) at a given total concentration of the ligand with the analogous, maximum capacity of the cement. Values collected at $\log([ISA]_{tot}/M) < 3.5$ fall within the range of experimental ζ potentials reported in the literature for analogous systems (represented in the figure by the shaded blue area) in the absence of any complexing ligand as adapted from (Pointeau et al., 2006b).

A clear decrease of the ζ potential occurs above $\log([ISA]_{tot}/M) \approx 3.5$, resulting in an isoelectric point at $\log([ISA]_{tot}/M) \approx 2.5$. In view of the strong sorption of the ligand onto the HCP (see Section 3.2.1), the isoelectric point can be explained as an electrokinetic charge inversion caused by the coverage of the ligand on the cement surface and/or its accumulation within the surface and the shear plane. As proposed by Pointeau and co-workers (Pointeau et al., 2008), the sorption of the ligand likely proceeds via the formation of a ternary species involving Ca (e.g. >SOCaISA), although experimental validation of this hypothesis is still missing. We note also that the ζ potential is only a well-defined property at fixed conditions (pH, electrolyte concentration, temperature, etc.). Although chloride concentration raises together with increasing ISA concentration in the system (with $[Cl^-]_{max} = 0.01\ M$ at $[NaISA] = 0.01\ M$, as a result of the NaCl excess in the ISA stock solution), the overall impact of $[Cl^-]_{tot}$ on the ζ potential is expected to be negligible compared to the large effect of ISA. A much stronger interaction of ISA with the cement surface is anticipated on the basis of its high affinity towards Ca^{2+}, as well as its H-bonding capabilities. Siretanu and co-workers reported a decrease in the effective surface charge of Gibbsite particles at $[Cl^-]_{tot} > 0.02\ M$, whereas the inversion of the surface charge was only achieved at $[Cl^-]_{tot} = 0.2\ M$ (Siretanu et al., 2014).

The decreasing ISA solution concentration in contact with increasing amount of HCP displayed in Fig. 1 supports that the observed evolution of the ζ potential in the system is induced by the uptake of ISA onto cement, although the exact distribution of the ligand on sorption sites, within the Stern layer and in the electric double layer cannot be inferred.

3.3. Redox conditions

Table 4 summarizes the redox conditions in terms of $(pe + pH_c)$ values determined in all investigated HQ-, Sn(II)- and dithionite-buffered systems containing Pu in the absence and presence of ISA. No general trends were found as a function of $[ISA]_{tot}$ or S:L, and thus Table 4 provides averaged $(pe + pH_c)$ values and corresponding uncertainties (calculated as 3 times the standard deviation).

HQ imposes moderately reducing conditions where $(pe + pH_c)$ values are in excellent agreement with values reported for analogous
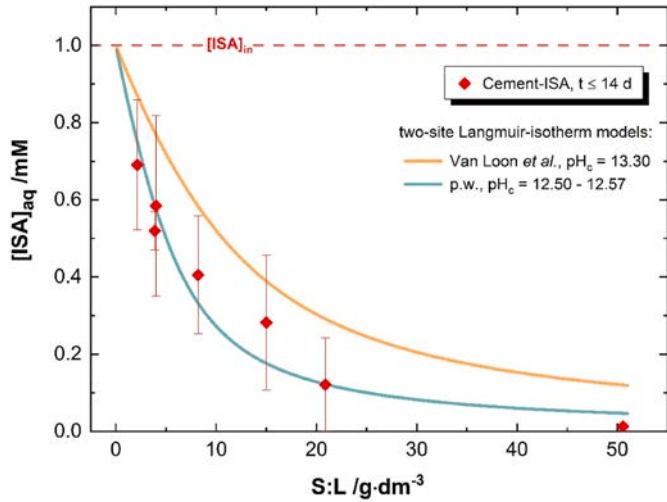
Fig. 1. Concentrations of ISA (red symbols) in pore water solutions with $pH_c = 12.50–12.57$ in equilibrium with the initial cement powder at log $([ISA]_{tot}/M) = −3$ (red, dashed line) and S:L of 2, 4, 8, 15, 20 and 50 g·dm$^{−3}$ at $t ≤ 14$ days. Solid lines represent the calculated concentrations using the two-site Langmuir-isotherm models based on: (i) orange: the data reported by Van Loon et al. (Van Loon and Glaus, 1998; Van Loon et al., 1997) and (ii) cyan: the results from the combined modelling approach performed on the data set of the present work with values from Equation (6). (For interpretation of the references to colour in this figure legend, the reader is referred to the Web version of this article.)

Pu–ISA systems in the absence of cement (Tasi et al., 2018a, 2018c). These (pe + pH$_c$) values fall within the stability field of Pu(IV), and thus the HQ systems are taken as references to investigate the cement–Pu(IV) and cement–Pu(IV)–ISA systems. NPOC measurements revealed no uptake of HQ by cement.

Sorption data collected in the presence of Sn(II) are taken as representative of more reducing conditions expected to develop in the post-closure period of deep geological repositories. Dithionite-buffered experiments are taken as analogues of the Sn(II)-buffered system in terms
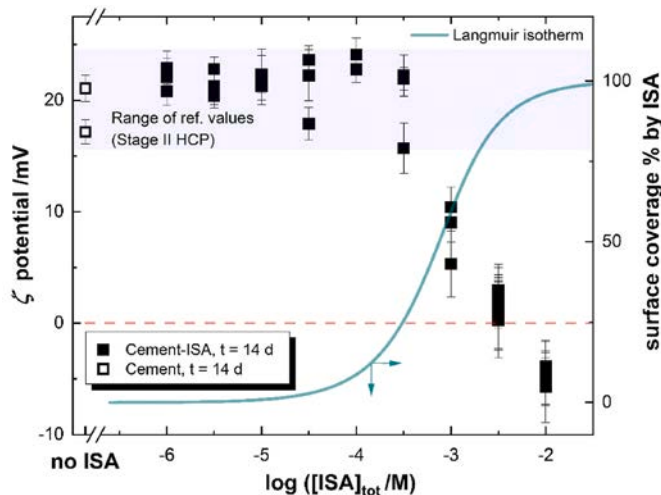
Fig. 2. Zeta-potentials (ζ) measured on suspended colloidal cement particles (at $pH_c = 12.50–12.63$) in the absence (opened symbols) and in the presence of ISA (filled symbols) with $−6 ≤ log ([ISA]_{tot}/M) ≤ −2$ in equilibrium with the initial cement powder at S:L = 4 g·dm$^{−3}$ after a contact time of t = 14 d. Solid cyan line represents surface coverage percentage of the cement solid phase by ISA as calculated from the two-site Langmuir isotherm established in the present work. (For interpretation of the references to colour in this figure legend, the reader is referred to the Web version of this article.)

Table 4
Average pH_c, pe and (pe + pH$_c$) values determined in all HQ-, Sn(II)- and dithionite-buffered batch sorption experiments containing Pu and in the absence and presence of ISA. Uncertainties are calculated as three times the standard deviation of the mean value.

Redox buffer (2 mM)	$pH_{c,av.}$	$pe_{av.}$	$(pe + pH_c)_{av.}$
HQ	(12.54 ± 0.16)	–(3.5 ± 1.0)	(9.2 ± 0.8)
Sn(II)	(12.50 ± 0.16)	–(11.6 ± 1.1)	(1.0 ± 0.7)
$S_2O_4^{2-}$	(12.50 ± 0.17)	–(12.4 ± 1.3)	–(0.3 ± 0.6)

of (pe + pH$_c$) values, whilst (due to their different chemical properties) providing a way to test the possible impact of the reducing chemicals on the sorption behavior.

3.4. Cement–Pu system

Fig. 3 shows the total aqueous concentrations of Pu in HQ-buffered pore water solutions contact with cement at 0.1 g·dm$^{−3}$ ≤ S:L ≤ 4.5 g·dm$^{−3}$. The figure summarizes the results obtained with two initial Pu concentrations, log ([Pu]$_{in}$/M) ≈ −5.3 (high oversaturation conditions, with respect to PuO$_2$(am,hyd)) and −8.3 (low oversaturation conditions), and contact times t ≈ 7–98 days. The figure includes the solubility of PuO$_2$(am,hyd) at pH_c ≈ 12.60 and associated uncertainty calculated using thermodynamic data reported in NEA-TDB (Guillaumont et al., 2003).
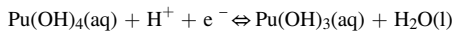
The systems with higher initial total concentrations of Pu (log ([Pu]$_{in}$/M) ≈ −5.3) show a gradual decrease in log ([Pu]$_{aq}$/M) values (≈ −10 at t ≈ 7 days, ≈ −11.5 at t ≈ 66 and 98 days). The final Pu concentrations are slightly lower but within the uncertainty of the calculated solubility of PuO$_2$(am,hyd), indicating the likely precipitation of Pu(IV) in this systems. This hypothesis is further supported by the slow decrease of Pu concentration, in contrast to the fast kinetics expected for sorption phenomena in cementitious systems (t ≤ 5 days) (Tits and Wieland, 2018).
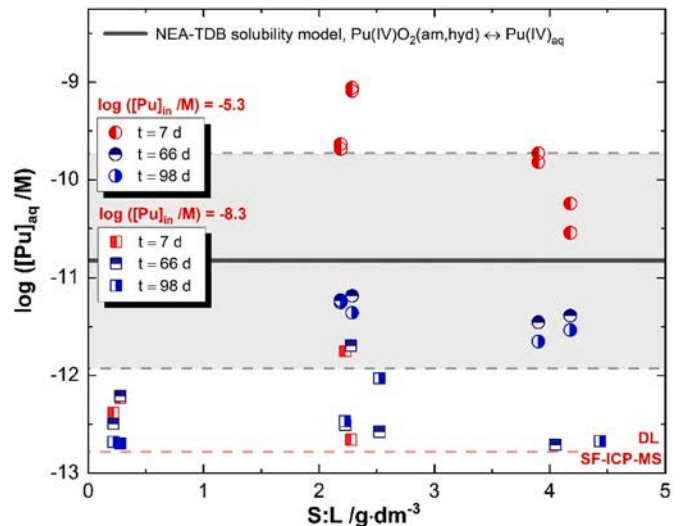
Fig. 3. Aqueous total concentrations of Pu quantified after centrifugation or ultrafiltration in HQ-buffered cement powder – pore water systems at t = 7 d (red), 66 d (dark blue) and 98 d (blue symbols) with S:L of ~0.2, ~2 and ~4 g dm$^{−3}$. Applied initial Pu concentration log ([Pu]$_{in}$/M) = −5.3 (half-filled circle symbols) and −8.3 (half-filled square symbols). Solid, black line and shaded area correspond to the solubility of PuO$_2$(am,hyd) in equilibrium with Pu(IV)$_{aq}$ species and its associated uncertainty, respectively. Calculations were made for pore water conditions (at pH_c = 12.60) using thermodynamic data reported in NEA-TDB (Guillaumont et al., 2003). (For interpretation of the references to colour in this figure legend, the reader is referred to the Web version of this article.)

On the other hand, the systems with log ([Pu]$_{in}$/M) $\geq$ 8.3 show a fast decrease in Pu liquid phase concentrations to log ([Pu]$_{aq}$/M) $\approx$ 12.5. This value is well below the solubility limit of PuO$_2$(am, hyd), and also clearly below the final concentration of Pu measured in systems with log ([Pu]$_{in}$/M) $\leq$ 5.3. These observations support the idea that the process driving the retention of Pu is different in systems with log ([Pu]$_{in}$/M) $\leq$ 5.3 and log ([Pu]$_{in}$/M) $\geq$ 8.3, with sorption controlling Pu concentration in the latter case.

No significant differences were observed between the Pu concentrations measured in sorption samples prepared with the same log ([Pu]$_{in}$/M) and S:L but different reducing agents applied (HQ, Sn(II) or dithionite) (data not shown). Considering that Pu is predominant in the +IV oxidation state in HQ-buffered systems, these observations suggest that (i) the fraction of Pu(III)$_{aq}$ in Sn(II) and Na$_2$S$_2$O$_4$ systems with much lower redox potential than in HQ is negligible compared to the total Pu concentration in solution; (ii) uptake of Pu(III)$_{aq}$ cannot be distinguished from that of Pu(IV)$_{aq}$, or (iii) both (i) and (ii). The low Pu concentrations remaining in solution after sorption ($\approx$10$^{-12.5}$ M) do not allow a reliable determination of the Pu redox speciation by any currently available analytical technique. As expressed from the redox and hydrolysis reaction equilibria, required reducing conditions for the redox transformation reaction between Pu(III)- and (IV)-hydroxo species follows the equation of:

$$Pu(OH)_4(aq) + H^+ + e^- \Leftrightarrow Pu(OH)_3(aq) + H_2O(l)$$

The rather large associated uncertainty is mainly due to the low Pu concentrations in solution, which are close to the detection limit even of the powerful quantification method (SF–ICP–MS) used in this work. This R$_d$ value is taken as reference for the uptake of Pu(IV) by cement CEM I in degradation stage II and under absence of ISA. The latter distribution ratio is slightly higher but in line with R$_d$ values reported in the literature for the uptake of An(IV) by analogous cementitious materials and C–S–H phases with C:S $\geq$ 1.5 (corresponding to cement degradation stage II) ((Baston et al., 1995; Tits et al., 2014b; Tits and Wieland, 2018; Wieland, 2014); among others).

3.5. Cement-Pu-ISA system

3.5.1. Solubility experiments with PuO$_2$(ncr,hyd) and ISA in cement pore water systems

Fig. 4 shows the total Pu concentrations as a function of log ([ISA]$_{tot}$/M) for 54 days, as well as the solubility curve of PuO$_2$(ncr,hyd) in the conditions of this experiment calculated using the thermodynamic model derived in Tasi et al. (2018a, 2018b). These experiments aimed at providing solubility upper limits to be considered in the sorption experiments, as well as to generate ISA-containing pore water solutions to be contacted with the initial cement powder in the course of the kinetic sorption experiments (see Section 3.5.3).

The model calculations slightly overestimate the solubility of Pu, but match well the trend observed with increasing ISA concentrations. Similar deviations of the thermodynamic model also occurred at

$$\log {}^*K°_{IVaq/IIIaq} \quad \log a_{Pu(OH)3(aq)} + \log a_w - \log a_{Pu(OH)4(aq)} + pH + pe \quad (0.0 \pm 0.7). \tag{7}$$

pH$_c$ $\geq$ 12.5 in Tasi et al. (2018b). These results confirm that the model available for the system Ca(II)–Pu(IV)–OH–ISA provides robust
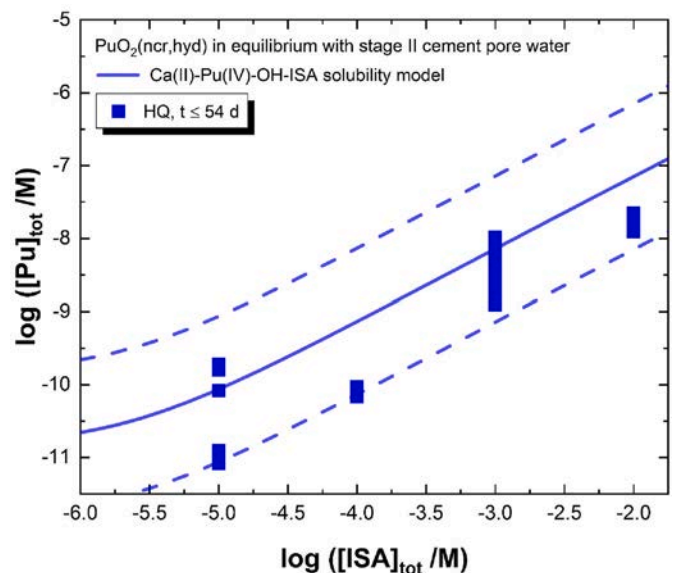
Considering the experimentally measured (pe + pH$_c$) values of (1.0 $\pm$ 0.7) (Sn(II) systems) and –(0.3 $\pm$ 0.6) (Na$_2$S$_2$O$_4$ systems), thermodynamic calculations do not provide unambiguous insight on the redox speciation expected for Pu$_{aq}$ in Sn(II) and S$_2$O$_4^{2-}$ systems. With regard to argument (ii), we note further that identical R$_d$ values were proposed for An(IV) and An(III) in the NAGRA sorption database for the cementitious near field of L/ILW repositories (100 m^3·kg^{-1}, degradation stage II) (Wieland, 2014).

The characterization of the oxidation state of Pu in the solid phase by XPS and XANES was only feasible for the more concentrated systems with log ([Pu]$_{in}$/M) $\geq$ 5.3, due to detection limit issues. In line with the main observations reflected in Fig. 3 for this initial concentration of Pu, XPS supports the presence of a Pu solid phase in HQ-buffered systems. XANES data confirm the predominance of Pu(IV) under these only mildly reducing conditions, whereas a mixture of Pu(IV) and Pu(III) (with $\approx$30% of the +III oxidation state) is observed for the Sn(II) systems (see Section SI-2.2.2 in the Supplementary Information).

Based on the discussion above, R$_d$ values were only calculated for those sorption systems with log ([Pu]$_{in}$/M) $\geq$ 8.3. Systematically higher R$_d$ values (1–1.5 log$_{10}$-units) were obtained from the sorption experiments with lower S:L ($\approx$0.2 g·dm^{-3}). This observation is in agreement with previous experimental findings reported for the analogous Th(IV) system (Wieland, 2014). At low S:L, R$_d$ values are more sensitive to factors such as the sorption of the radionuclide onto the vessel walls, or inhomogeneity of the cement powder. On the other hand, consistent R$_d$ values are obtained for the systems with S: L 2–4 g·dm^{-3}. An average value calculated for data collected in HQ-systems with log ([Pu]$_{in}$/M) $\geq$ 8.3 results in:

$$\log (R_{d,in} /dm^3·kg^{-1}) \quad (6.3 \pm 0.6). \tag{8}$$

Fig. 4. Total concentrations of Pu quantified after ultrafiltration in HQ-buffered pore water solutions with t $\leq$ 54 d at 5 $\leq$ log ([ISA]$_{tot}$/M) $\leq$ 2 in equilibrium with PuO$_2$(ncr,hyd) solid phase (in the absence of HCP). Solid (and dashed) blue curve line corresponds to the solubility of PuO$_2$(ncr,hyd) under pore water conditions in the presence of ISA and Ca(II) (and its related uncertainties), calculated using the thermodynamic and SIT activity models reported in Tasi et al. (2018a, 2018b). (For interpretation of the references to colour in this figure legend, the reader is referred to the Web version of this article.)
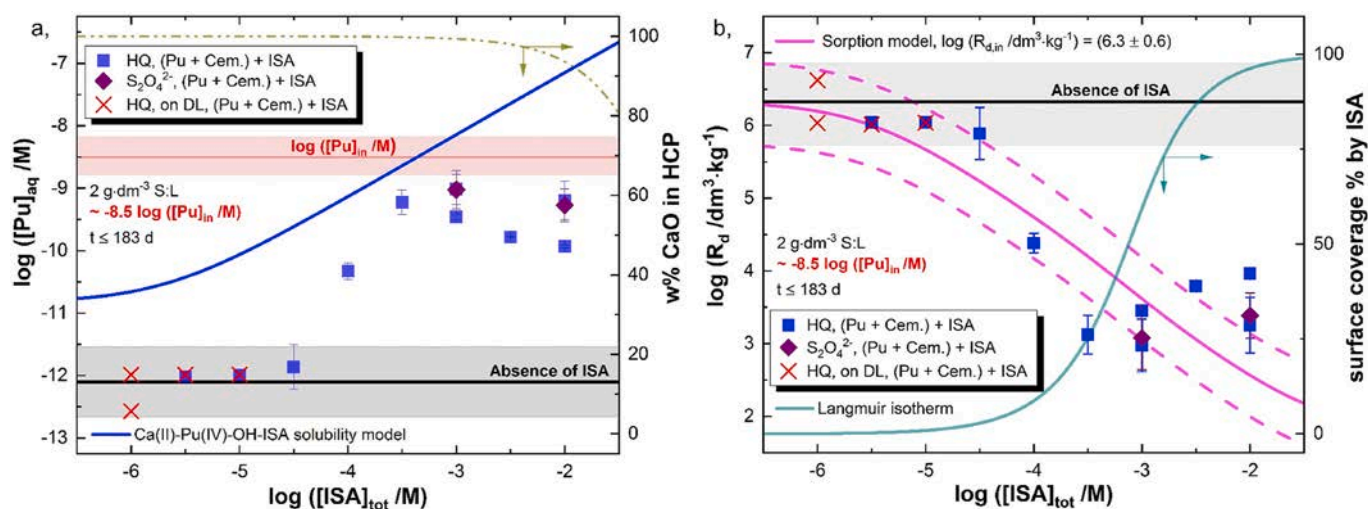
Fig. 5. (a) Aqueous total concentrations (M), and (b) Distribution ratios (dm^3·kg^{-1}) of Pu in HQ- (blue) and dithionate-buffered (purple symbols) cement powder – pore water systems with log ([Pu]$_{in}$/M) ≈ 8.5, 6 ≤ log ([ISA]$_{tot}$/M) ≤ 2 and S:L = 2 g·dm^{3} for the sequence in the order of addition of individual components: "(Pu + Cement) + ISA". Solid blue line corresponds to the solubility of PuO$_2$(ncr,hyd) within the boundary conditions of the experiments, calculated using the thermodynamic and SIT activity models reported in (Tasi et al., 2018b). Solid black line and gray shaded area indicate the expected values of the distribution coefficient of Pu or [Pu]$_{aq}$ (and uncertainty) in the absence of ISA according to log (R$_{d,in}$/dm^3·kg^{-1}) = (6.3 ± 0.6). Violet solid (and dashed) line shows the calculations of the simplified sorption model for the conditions of this experiment (and associated uncertainties). Dashed-dotted line indicates the calculated stability limit of HCP expressed in terms of percentage of CaO present in HCP (scale on the right y-axis). Solid cyan line represents surface coverage percentage of the cement solid phase by ISA as calculated from the two-site Langmuir isotherm established in the present work. (For interpretation of the references to colour in this figure legend, the reader is referred to the Web version of this article.)

solubility limits under pore water conditions.

3.5.2. Sorption and desorption experiments

The effect of the order of addition of the individual components (cement/Pu/ISA) on the sorption process was evaluated at two ISA total concentrations: log ([ISA]$_{tot}$/M) 3 and 2. Differences in the results reflect the absence of thermodynamic equilibrium for the addition sequence of "(Pu + ISA) + cement" within the timeframe of the experiments (t ≤ 183 d). In this regard, the present section is entirely dedicated to discuss equilibrium state results of sorption experiments (those corresponding to "(Pu + cement) + ISA" addition sequence), whereas findings of kinetic investigations (experiments conducted following the addition sequence "(Pu + ISA) + Cement", or coupled to the undersaturation solubility systems) are detailed in Section 3.5.3.

In all cases, experimental sorption data are compared to solubility calculations using the chemical and thermodynamic models derived in Tasi et al. (2018a, 2018b) providing upper limits for the concentration of Pu in the presence of ISA. Evaluation of the data obtained for the ternary systems cement-Pu-ISA with log ([Pu]$_{in}$/M) 5.8 suggests a solubility control of the Pu aqueous concentrations (see Supplementary Information, SI-2.3.1), and thus have no relevance in the context of sorption phenomena. XANES analysis of the oxidation state of plutonium in this system confirms the predominance of Pu(IV), in line with our previous study for the system Ca–Pu–ISA in the absence of cement (Tasi et al., 2018a, b).

Fig. 5 summarizes the results of the "(Pu + cement) + ISA" sorption experiments for systems with S:L 2 g·dm^{-3}, log ([Pu]$_{in}$/M) 8.5 and 6 ≤ log ([ISA]$_{tot}$/M) ≤ 2, expressed as log ([Pu]$_{aq}$/M) *vs.* log ([ISA]$_{tot}$/M) (figure a) and log (R$_d$/dm^3·kg^{-1}) *vs.* log ([ISA]$_{tot}$/M) (figure b). Fig. 5a shows also the calculated stability limit of HCP expressed in

terms of % CaO present in HCP.[1] This estimation indicates that within the boundary conditions of these experiments (S:L 2 g·dm^{-3}, –6 ≤ log ([ISA]$_{tot}$/M) ≤ 2), only a minor fraction of cement is dissolved by the effect of ISA. Analogous experiments conducted with S:L 0.2 g·dm^{-3}, log ([ISA]$_{tot}$/M) 3 and 2 are subjected to a significant dissolution of the HCP, and hence, the results are only summarized in the Supplementary Information (SI-2.3.1). In figure b the surface coverage of HCP by ISA in percentages as a function of ISA total concentration (cyan solid line) is also attached as derived from the Langmuir isotherm using values from Equation (6).

Fig. 5a shows that Pu concentrations in systems with S:L 2 g·dm^{-3} are well below the solubility limit of PuO$_2$(ncr,hyd) in the presence of ISA (solid blue line). Thus, results of experiments with log ([Pu]$_{in}$/M) 8.5 clearly relate to sorption phenomena and are not controlled by solubility with regard to PuO$_2$(am,hyd). The concentration of Pu remains remarkably low (≈10^{-12} M) up to log ([ISA]$_{tot}$/M) 4.0, indicating that Pu sorption is not or rather less affected below this ISA concentration. Fig. 5a shows also virtually the same results for experiments in HQ- (pe + pH$_c$ ≈ 9) and S$_2$O$_4^{2-}$ (pe + pH$_c$ ≈ 0.3) buffered systems. In line with experimental observation in analogous systems made in the absence of cement (Tasi et al., 2018a, b), these results support the predominance of Pu(IV) in all evaluated cement systems in the presence of ISA.

All values of log (R$_d$/dm^3·kg^{-1}) determined at log ([ISA]$_{tot}$/M) ≤ 4.5, partially located on the detection limit, fall within the range of the initial value: log (R$_{d,in}$/dm^3·kg^{-1}) (6.3 ± 0.6), underlining the validity of the distribution ratio quantified in the absence of ISA. At log ([ISA]$_{tot}$/M) > 4.5, the clear decrease in R$_d$ values is caused by the stronger competition of aqueous complex formation reactions towards Pu(IV), mobilizing Pu surface species in the form of quaternary Ca(II)–

---

[1] Calculated by subtracting the amount of calcium ions dissolved as Ca–ISA complexes (*i.e.* differential of calcium concentration above 0.021 M) to the molar amount of CaO available in the cement. The latter value is calculated considering the molar fraction of CaO in the hydrated cement, the weight of cement and the S:L applied.

Pu(IV)–OH–ISA species. This tendency however, reverses at log ([ISA]$_{tot}$/M) $\geq$ 3.5, and a slight but systematic increase in the R$_d$ values is observed above this ISA concentration, up to log ([ISA]$_{tot}$/M) 2. This effect correlates with the trend in measured ζ potentials of suspended HCP particles, for which decreasing positive values and a charge inversion are observed at log ([ISA]$_{tot}$/M) > 3.5 (see cyan line as well in Fig. 5b). Under those conditions, the coverage of cationic HCP sites with ISA approaches saturation (see also (Van Loon et al., 1997)). Hence, co-adsorption of Pu(IV) with ISA onto HCP, likely in the form of stable surface complex(es) can be assumed.

Although a surface complexation implemented diffuse layer model (SCM-DLM) usually estimates surface potentials on solid–liquid interfaces reasonably well, it necessitates the knowledge of a large number of surface properties of the adsorbate and the mechanistic insight into prevailing surface equilibria. Considering the limited structural information available on C–S–H phases and the insufficient performance of any technique on Pu speciation analysis at the extreme low concentration level of the present system, most parameters of an anticipated model (such as types and densities of sorption sites, surface species) would have to be assumed. In this regard, the description of the system can be better approached from the side of the dominant aqueous complexation reactions in the system. In order to account for the decreased sorption with increasing ISA concentration, a *simplified sorption model* can be set up, where the given effect is exclusively attributed to the formation of the Pu(IV)–OH-ISA and Ca(II)-Pu(IV)–OH-ISA aqueous complexes. The *simplified sorption model* follows the method described by Schubert for ion exchange materials (Schubert, 1948), which has been extensively applied for the determination of complexation constants in radionuclide–organic systems of relevance for nuclear waste disposal (Rojo et al., 2013; Tits et al., 2005; Vercammen, 2000; Vercammen et al., 2001). Analogous sorption models are also considered in the determination of the sorption reduction factors (SRF, F$_{red}$), a quantity often used in Safety Analysis to evaluate the impact of perturbing factors (*e.g.* complexing ligands) on radionuclide mobility (Bruno et al., 2018; SKB, 2008; Tits et al., 2002; Van Loon and Glaus, 1998; Wieland, 2014).

The application of the *simplified sorption model* requires that the sorption of the metal ion (*e.g.* Pu^{4+}) within the range of conditions investigated is linear, reversible and non-competitive towards any other species in solution. It also assumes that the aqueous complexes (*e.g.* Ca(II)–Pu(IV)–ISA) do not sorb onto the solid phase. This model is undoubtedly an oversimplification of the Pu retention process, and thus, it is considered for a semi-quantitative comparison with experimental data. The *simplified sorption model* can be expressed as described in Equation (9):

$$\log R_d \quad \log R_{d,in} - \log (1 + {}^*\beta'_{1,4,1}\cdot[ISA^-]_{free}\cdot(A\cdot[H^+]^4)^{-1} + {}^*\beta'_{1,5,1}\cdot[ISA^-]_{free}\cdot(A\cdot[H^+]^5)^{-1} +.$$

$$+ {}^*\beta'_{1,1,4,1}\cdot[ISA^-]_{free}\cdot[Ca^{2+}]_{free}\cdot(A\cdot[H^+]^4)^{-1} + {}^*\beta'_{1,1,5,1}\cdot[ISA^-]_{free}\cdot[Ca^{2+}]_{free}\cdot(A\cdot[H^+]^5)^{-1}), \quad (9)$$

where log (R$_d$/dm^3·kg^{-1}) (6.3 ± 0.6) as determined in this work in the absence of ISA, ${}^*\beta'_{1,n,1}$, and ${}^*\beta'_{1,1,n,1}$ (with n 5 or 6) are the conditional equilibrium constants for the formation of the ternary and quaternary complexes Ca(II)-Pu(IV)–OH-ISA as derived in (Tasi et al., 2018a, b). The A is the term accounting for the hydrolysis species of Pu(IV) prevailing in the investigated pore water conditions:

$$A \quad 1 + {}^*\beta'_{1,4}\cdot[H^+]^{-4}, \quad (10)$$

where ${}^*\beta'_{1,4}$ is the conditional equilibrium constant for the formation of Pu(OH)$_4$(aq). The free proton concentration in solution was calculated from the experimentally determined pH$_c$ values, whereas the free concentrations of Ca^{2+} and ISA$^-$ ions were obtained from Equations (11) and (12), respectively.

$$[Ca]_{tot} \quad [Ca^{2+}]_{free} + [CaOH^+] + [CaISA^+] + [CaISA^0_H] + [Ca_4Pu(OH)_8^{4+}] +$$

$$+ [CaPu(OH)_3ISA^+_H] + [CaPu(OH)_3ISA^0_{2H}] \quad 0.02\,M \quad (11)$$

$$[ISA]_{aq} \quad [ISA^-]_{free} + [CaISA^+] + [CaISA^0_H] + [Pu(OH)_3ISA^-_H] + [Pu(OH)_3ISA^{2-}_{2H}] + [CaPu(OH)_3ISA^+_H] + [CaPu(OH)_3ISA^0_{2H}] \quad (12)$$

The contribution of all Pu-bearing species to [Ca]$_{tot}$ and [ISA]$_{aq}$ is negligible and was disregarded in the final calculations. Formation constants were corrected for the ionic strength in the pore water solutions using the SIT formalism (Tasi et al., 2018b). The values of [ISA]$_{aq}$ were calculated on the basis of the initial ligand concentration also considering the two-site Langmuir-isotherm described in Section 3.2.1.

Predicted log (R$_d$/dm^3·kg^{-1}) values calculated by the *simplified sorption model* (solid and dashed violet curve) are attached in Fig. 5b showing the decrease of the uptake of Pu by HCP as a function of log ([ISA]$_{tot}$/M) at S:L 2 g·dm^{-3}.

Although a striking similarity between the trends of model calculations and experimentally determined distribution ratios can be instantly identified, an accurate description of the data set is not achieved. As the model does not consider the sorption of Ca(II)–Pu(IV)–OH–ISA complexes on the cement surface above the level of log ([ISA]$_{tot}$/M) > 3.5, it is evident that it systematically fails at explaining the given increase in log (R$_d$/dm^3·kg^{-1}) values. The mismatch observed below log ([ISA]$_{tot}$/M) < 3 however, could be due to different reasons: i, wrongly adapted Pu solution speciation; ii, not independent sorption behavior of aqueous species of Pu and ISA. In the *simplified sorption model*, the decrease in log (R$_d$/dm^3·kg^{-1}) values detected between log ([ISA]$_{tot}$/M) 4.5 and 3.5 is only attributed to the competition between sorbed Pu and the formation of Ca–Pu–ISA aqueous complexes. Consequently, the trend in the decrease of log (R$_d$/dm^3·kg^{-1}) vs. log ([ISA]$_{tot}$/M) (slope) is directly correlated to the stoichiometric ratio of Pu to ISA in the aqueous Ca–Pu–ISA complex. However, experimental log (R$_d$/dm^3·kg^{-1}) values vs. log ([ISA]$_{tot}$/M) follow a much steeper decrease than the one predicted by the *simplified sorption model* (see Fig. 5b), suggesting the predominance of different ternary Ca–Pu–ISA complexes than those
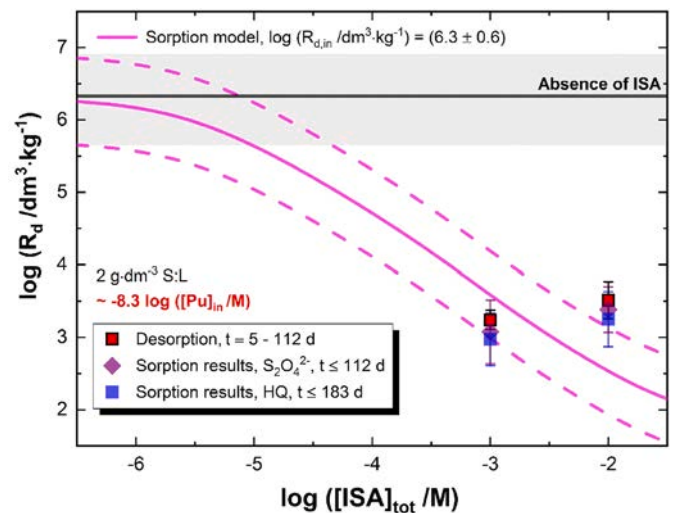

Fig. 6. Distribution ratios (R$_d$ values in dm^3·kg^{-1}) of Pu determined in desorption experiments in HQ-buffered cement powder – pore water systems at S:L ≈ 2 g·dm^{-3}, log ([Pu]$_{in}$/M) 8.3 and log ([ISA]$_{tot}$/M) 3 and 2 (red rectangles, with t = 5–112 d). Blue and purple symbols show sorption data obtained under the same boundary conditions in the presence of HQ and dithionite buffers, respectively. Violet curves (solid and dashed) correspond to the log (R$_d$/dm^3·kg^{-1}) values (and uncertainties) calculated with the simplified sorption model. (For interpretation of the references to colour in this figure legend, the reader is referred to the Web version of this article.)

proposed from solubility experiments (Tasi et al., 2018b). The re-evaluation of sorption data on the basis of the *simplified sorption model* assuming different Pu solution speciation (see Supplementary Information, SI-2.3.2) underlines that a full consistency between the latter trend in sorption data and the reliable prediction of the solubility data set cannot be simultaneously achieved. The discrepancy between the models reflects the complexity of the system, *i.e.* not all assumptions of the simplified model are valid and puts the possible competitive nature between the sorption processes of Pu and ISA in front.

In light of evidence on the strong, preferential uptake of ISA by C-A-S-H phases (Van Loon and Glaus, 1998), at low S:L applied, total saturation of aluminate-type sorption sites in the hydrated cement phase by ISA can be readily expected at relatively low log ([ISA]$_{tot}$/M). In case an analogous sorption mechanism for Pu(IV) prevails, the specific adsorption of ISA by C-A-S-H phases would impose a significant decrease in the site accessibility for plutonium with log ([Pu]$_{in}$/M) 8.5. As a consequence, this could cause a more rapid decrease in equilibrium values of log (R$_d$/dm^3·kg^{-1}) as a function of increasing log ([ISA]$_{tot}$/M) than it is solely attributed to solution complexation effects. The role of C-A-S-H phases in the uptake of Pu is however, yet unknown and numerous experimental studies (Aggarwal et al., 2000; Gaona et al., 2011; Pointeau et al., 2004; Tits et al., 2014a, 2014b) postulate rather the more abundant C–S–H phases (with associated silanol groups) to be the main sink for tri- and tetravalent actinides. Note also that uncertainties in the quantification of Pu distribution ratios at the extremely low concentration levels dictated by the boundary conditions are rather high and exceed the displayed ranges attached to the data points in Fig. 5. Hence, a final conclusion on the sorption mechanism cannot be drawn at this stage.

To assess the reversibility of the uptake process, desorption experiments were executed by introducing ISA-containing ([ISA]$_{tot}$ 10^{-3} and 10^{-2} M) pore water solutions onto equilibrated cement phases retrieved from the binary sorption experiments (absence of ISA, log ([Pu]$_{in}$/M) ≈ 8.5, S:L ≈ 2 g·dm^{-3}). Fig. 6 shows the log (R$_d$/dm^3·kg^{-1}) values determined for these desorption samples at *t* 5–112 days (red squares). The figure also includes log (R$_d$/dm^3·kg^{-1}) values determined in *sorption* experiments

conducted under the same boundary conditions and following the sequence "(Pu + Cement) + ISA" (HQ- and dithionite-buffered samples indicated by blue and purple symbols, respectively). The solid (violet) line represents the *simplified sorption model* as described before.

In the presence of ISA in solution, desorption resulted in fast equilibration, with stable log ([Pu]$_{aq}$/M) values quantified after 5 days of contact time. Furthermore, the desorption experiments confirm the previously identified stronger uptake (*i.e.* higher R$_d$ values) at log ([ISA]$_{tot}$/M) 2 than for log ([ISA]$_{tot}$/M) 3. Results of desorption experiments show log (R$_d$/dm^3·kg^{-1}) values in excellent agreement with sorption data obtained following the sequence "(Pu + Cement) + ISA". The latter observation underlines that these values correspond to equilibrium conditions within the system.

3.5.3. Kinetic effects

Interesting features of our experiments performed with high and low [Pu]$_{in}$ refer to the substantially different behavior observed as a function of the order of addition, *i.e.* much higher solution concentrations of Pu are observed for the sequence "(Pu + ISA) + Cement". In this case, for both initial Pu concentrations: log ([Pu]$_{in}$/M) 5.8 and 8.5, metal ion concentration remains practically unchanged during contact with cement for ≤ 109 and ≤ 183 d, respectively (see Figures SI-8 a, b and SI-10). In both cases, the expected equilibrium state does not establish for the sequence "(Pu + ISA) + Cement". The most likely explanation for these experimental findings is the high kinetic inertness of the dominant ternary and quaternary complexes Ca(II)–Pu(IV)–OH–ISA forming in the aqueous phase.

In comparison with the equilibrium sorption results, the higher Pu concentrations (*i.e.* "weaker" uptake) observed for the sequence "(Pu + ISA) + Cement" are most obvious for S:L 2 g·dm^{-3} and log ([Pu]$_{in}$/M) 8.5 conditions (see Fig. SI-10 in Supplementary Information). Indeed, Pu concentrations measured for the latter case are rather close to the initial Pu concentration introduced to the system. Under comparable conditions, Baston et al. (1995) investigated the uptake of Pu(IV) by cementitious materials (concrete, mortar), where log ([ISA]$_{tot}$/M) 2.7 and S:L 20 g·dm^{-3} applied. Although, not explicitly
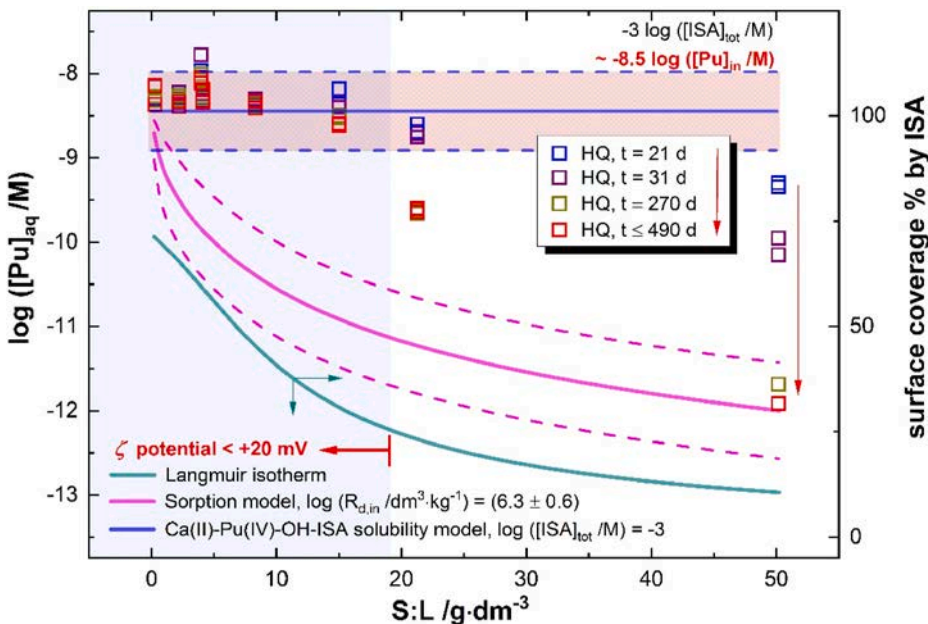

Fig. 7. Aqueous total concentrations of Pu quantified after 10 kDa ultrafiltration at t$_{eq}$ ≤ 490 d in HQ-buffered (blue symbols) cement powder – pore water systems with log ([ISA]$_{tot}$/M) = 3 and 0.2 g·dm^{-3} ≤ S:L ≤ 50 g·dm^{-3}. Aqueous solutions contacted with cement are the supernatant of undersaturation solubility experiments with PuO$_2$(ncr,hyd) as described in Section 3.5.1, resulting in log ([Pu]$_{in}$/M) = –(8.5 ± 0.5) (solid and dashed blue lines). Violet curves (solid and dashed) correspond to the log ([Pu]$_{aq}$/M) calculated with the simplified sorption model considering the decrease of log ([ISA]$_{aq}$/M) with increasing S:L (considering uncertainties). Orange curve represents surface coverage percentage of the cement solid phase by ISA as calculated from the two-site Langmuir isotherm established in the present work using values from Equation (6). (For interpretation of the references to colour in this figure legend, the reader is referred to the web version of this article.)

stated in the work, their experiments involving ISA expectedly followed the sequence "(Pu + ISA) + Cement". The authors reported log ($R_{d, in}$/dm^3·kg^{-1}) $\approx$ 6.1–6.8 (concrete and mortar) in the absence of ISA, and log (R_d/dm^3·kg^{-1}) $\approx$ 2.1–2.3 (concrete) for log ([ISA]$_{tot}$/M) 2.7 (contact time not reported). Distribution ratios quantified in the absence of ISA are in line with those obtained in the present work, whereas log (R_d/dm^3·kg^{-1}) values in the presence of ISA are, indeed, consistent with the results obtained in this study for the sequence "(Pu + ISA) + Cement".

For the purpose of capturing the evolution of [Pu]$_{aq}$ in the transient state encountered by following the addition sequence "(Pu + ISA) + Cement", the supernatant solutions from undersaturation solubility experiments were separated from the solid phase (PuO$_2$(ncr,hyd)), and contacted with increasing amounts of cement powder. At this level of ISA total concentration, the increase in S:L parameter translates into a significant decrease in the percentage of ISA-coverage of the cement surface (from $\approx$70 to $\approx$10%). This provides more available surface sites for the uptake of Pu, whilst still maintaining sufficiently high ISA concentrations (log ([ISA]$_{aq}$/M) 3 to 4.3) to induce a visible decrease in Pu retention. Note also that much longer contact times were considered for the equilibration of these systems (t $\leq$ 490 d), compared to the standard sorption experiments following the sequence "(Pu + ISA) + Cement" (t $\leq$ 183 d).

Fig. 7 shows the results of this series of sorption experiments expressed as log ([Pu]$_{aq}$/M) *vs.* S:L. The figure also contains the surface coverage of HCP by ISA in percentages as a function of S:L (cyan solid line, right y-axis) calculated from the Langmuir isotherm using values from Equation (6). The values of log ([Pu]$_{aq}$/M) calculated using the *simplified sorption model* considering the decrease in log ([ISA]$_{aq}$/M) with increasing S:L and uncertainties are shown as (solid and dashed) violet curves in Fig. 7.

For systems with S:L $\leq$ 8 g·dm^{-3}, Fig. 7 shows values of log ([Pu]$_{aq}$/M) $\approx$ log ([Pu]$_{in}$/M), even after 490 days of contact time. A minor decrease in log ([Pu]$_{aq}$/M) values is observed for S:L 15 g·dm^{-3} after 490 days, whereas the decrease in log ([Pu]$_{aq}$/M) becomes more pronounced above this S:L. For the highest S:L (50 g·dm^{-3}), the initial concentration of Pu decreases by almost four orders of magnitude within 490 days of contact time. The log ([Pu]$_{aq}$/M) measured after 400 days matches well the Pu concentration predicted by the *simplified sorption model*. Note, that for S:L 50 g·dm^{-3} (with log ([ISA]$_{aq}$/M) $\approx$ 4.3) a reasonable agreement between experimental data for the sequence "(Cement + Pu) + ISA" (at log ([ISA]$_{tot}$/M) $\approx$ 4.0) and also with the *simplified sorption model* was reached especially taking into account the expected high uncertainties in the system (see Fig. 5b).

A closer inspection of the kinetic evolution of available data (S:L 20 and 50 g·dm^{-3} in Fig. 7) as a function of contact time reveals that the adsorption process follows a pseudo-second order degree equation. Substantial differences in the rate constants for the two systems also suggest a competitive sorption behavior existing between Pu(IV) and ISA. The presently available scarce amount of data however, does not allow us to draw a conclusion in this regard. Predictive calculations correlating empirical rate constants with the ISA-coverages of present HCP indicate that the contact time required to attain equilibrium conditions in systems with S:L $\leq$ 8 g·dm^{-3} and log ([ISA]$_{tot}$/M) $\geq$ 3.0 can be in the range of decades. Considering all evidence, the sequence "(Pu + Cement) + ISA" can be adapted as the fastest path to attain equilibrium conditions in the ternary system Cement–Pu–ISA. On the basis of the present study, previous results on the ternary system Cement–Pu–ISA may need to be revisited with the consideration of the

order of addition of the individual components. This can possibly be extended to other Cement–RN–organics systems, in which the cement offers an effective sink for the uptake of both the radionuclide and the organic ligand. In view of the applicability, extensive parameters such as S:L in the near field of a disposal facility are known to be at several orders of magnitude higher level, which could significantly alter the overall trends with respect to the effect of *"order of addition"* observed in small scale laboratory experiments. Hence, in relation to end-user application, future work aimed especially at achieving a better mechanistic insight into the processes controlling the *"order of addition"* effect is required.

4. Summary and conclusions

In the absence of ISA, cement in the degradation stage II sorbs Pu strongly under the reducing conditions investigated in this work (0 $\leq$ (pe + pH$_c$) $\leq$ 9). Distribution ratios determined for Pu are in line with sorption data available in the literature for tetravalent actinides.

The uptake of ISA by cement is substantial (log (R_d/dm^3·kg^{-1}) $\approx$ 2.6) and can be empirically described by a two-site Langmuir isotherm. Approaching the saturation of relevant HCP sorption sites induces a significant decrease in the zeta potential values of suspended cement particles at log ([ISA]$_{tot}$/M) $\geq$ 3.5 and S:L 4 g·dm^{-3} from positive to negative charges. Observations clearly point to the gradual change of HCP surface properties above ~25% of ISA-coverage.

Undersaturation solubility experiments conducted with PuO$_2$(ncr, hyd) in cement pore water (pH$_c$ $\approx$ 12.5, [Ca]$_{tot}$ 0.02 mol·dm^{-3}) and in the presence of 5 $\leq$ log ([ISA]$_{tot}$/M) $\leq$ 2 validate our previous thermodynamic model derived for the system Ca^{2+}–Pu^{3+}–Pu^{4+}–OH$^-$–Cl$^-$–ISA$^-$–H$_2$O(l) (Tasi et al., 2018a, b).

The uptake of Pu by cement importantly decreases above log ([ISA]$_{tot}$/M) $\approx$ 4.5. Analogous results are obtained for the different reducing systems investigated (HQ, Sn(II), Na$_2$S$_2$O$_4$), thus supporting that Pu(IV) predominates both as surface and aqueous complex. This is consistent with our previous studies in the absence of cement (Tasi et al., 2018a, b), and suggest a role of ISA in the stabilization of the +IV plutonium oxidation state in the ternary system cement-Pu-ISA as well. The surface uptake of Pu slowly increases again above log ([ISA]$_{tot}$/M) $\approx$ 3.5. This phenomenon is attributed to the co-adsorption of Pu (IV) with ISA, probably in the form of Ca(II)–Pu(IV)–OH–ISA surface complexes, which correlates well with the change in surface properties of suspended cement particles induced by the increasing total ISA concentration in solution.

The impact of the order of addition of the individual components (Pu/ISA/cement) on the sorption processes was investigated. Significant differences are found between the sequences *(Pu + Cement) + ISA* and *(Pu + ISA) + Cement,* with the former sequence showing systematically higher log (R_d/dm^3·kg^{-1}) values. Long-term sorption experiments (t $\leq$ 490 days) in combination with desorption experiments confirm significantly longer times for the sequence *(Pu + ISA) + Cement* to attain equilibrium. This is likely due to the kinetic inertness of the ternary/ quaternary Ca(II)–Pu(IV)–OH–ISA complexes forming in the aqueous phase. Additional systematic studies, especially aiming at deriving better mechanistic insight into the processes controlling the *"order of addition"* effect in cement-radionuclide-organic systems, are required in the future.

A *simplified sorption model* was derived on the basis that the decrease in the uptake of Pu by HCP is only caused by the formation of Ca(II)–Pu (IV)–OH–ISA aqueous complexes. Model predictions qualitatively agree

well with the trend in experimental data over a wide parameter-range but fails to account for the uptake of Pu above a certain level of ISA-coverage (>~25%) of the cement surface. A more in-detail examination of deviations between the model calculations and obtained data at low ISA concentrations revealed a competitive nature between the sorption processes of Pu(IV) and ISA onto HCP. The latter observation was also reflected in the kinetic experiments where a substantial difference in the rate constants for Pu(IV) sorption was obtained for different S:L at a constant ligand total concentration. As of now, the complexity of the system in combination with the missing scientific gaps in the description of sorption mechanism for Pu(IV) does not allow us to provide a conclusive sorption model. The underprediction of the log R_d values by the *simplified sorption model* at high ISA concentrations is admittedly unsatisfying from a scientific point of view but allows deriving robust upper limit concentrations of Pu for use in the applied context.

The present work demonstrates the substantial impact of ISA on Pu (IV) retention by HCP under mildly to strongly reducing conditions. The dataset provides a significantly improved basis for long-term predictions of Pu behavior in repositories for L/ILW containing cellulose. Beyond its practical implications, this study also provides arguments towards a better mechanistic understanding of the interactions driving sorption processes of actinides onto hydrated cement phases in the presence of specific organic ligands.

Declaration of competing interest

Acknowledgements

Appendix

Table A1
Thermodynamic data (at reference state) used for the solubility and hydrolysis equilibria calculations of Pu(IV), as adapted from (Neck et al., 2007) and (Guillaumont et al., 2003).

Chemical equilibrium	log K°
$PuO_2(am, hyd) \rightleftharpoons Pu^{4+} + 4\ OH$	–(58.33 ± 0.52)
$Pu^{4+} + OH \rightleftharpoons Pu(OH)^{3+}$	(14.6 ± 0.2)
$Pu^{4+} + 2\ OH \rightleftharpoons Pu(OH)_2^{2+}$	(28.6 ± 0.3)
$Pu^{4+} + 3\ OH \rightleftharpoons Pu(OH)_3^{+}$	(39.7 ± 0.4)
$Pu^{4+} + 4\ OH \rightleftharpoons Pu(OH)_4^{0}(aq)$	(47.5 ± 0.5)

Table A2
Complementary thermodynamic data (at reference state or otherwise indicated) for the system Ca(II)–OH–ISA reported in the literature and considered in the present work.

Chemical equilibrium	log K°	Reference
$HISA(aq) \rightleftharpoons HISA_L(aq) + H_2O(l)$	(0.5 ± 0.2)[a]	Rai and Kitamura (2015)
$H^+ + ISA^- \rightleftharpoons HISA(aq)$	(3.3 ± 0.2)[a]	Rai and Kitamura (2015)
$H^+ + ISA^2_{-H} \rightleftharpoons ISA^-$	14.31 (I ~ 2 M)	Evans (2003)
$Ca^{2+} + OH \rightleftharpoons Ca(OH)^+$	1.22	Blanc et al. (2010)
$Ca^{2+} + 2OH \rightleftharpoons Ca(OH)_2(s)$	−5.19	Blanc et al. (2010)
$Ca^{2+} + 2\ ISA^- \rightleftharpoons Ca(ISA)_2(s)$	(6.4 ± 0.2)	Hummel et al. (2005)
$Ca^{2+} + ISA^- \rightleftharpoons CaISA^+$	(1.7 ± 0.3)	Hummel et al. (2005)
$Ca^{2+} + ISA^- \rightleftharpoons CaOHISA(aq)^b + H^+$	–(10.4 ± 0.5)	Hummel et al. (2005)

[a] Uncertainties estimated in Hummel et al. (2005).
[b] Hummel and co-workers reported this species as $Ca(ISA_{-H})(aq)$ (Hummel et al., 2005).

Table A3
Chemical equilibria and related equilibrium constants (at I → 0 m) derived in our previous study for the Ca(II)–Pu(III/IV)–OH–ISA system (Tasi et al., 2018a, b).

Chemical equilibrium	log*β°
$Pu^{4+}(aq) + ISA^- + 3\ H_2O(l) \rightleftharpoons Pu(IV)(OH)_3ISA^-_{-H} + 4\ H^+$	–(5.03 ± 0.12)
$Pu^{4+}(aq) + ISA^- + 3\ H_2O(l) \rightleftharpoons Pu(IV)(OH)_3ISA^{2-}_{-2H} + 5\ H^+$	–(16.92 ± 0.13)
$Pu^{3+}(aq) + ISA^- + H_2O(l) \rightleftharpoons Pu(III)(OH)ISA_{-H}(aq) + 2\ H^+$	–(10.97 ± 0.28)
$Pu^{4+} + ISA^- + 4\ H_2O(l) + Ca^{2+} \rightleftharpoons Ca(II)Pu(IV)(OH)_3ISA^+_{-H} + 4\ H^+$	–(1.66 ± 0.10)
$Pu^{4+} + ISA^- + 5\ H_2O(l) + Ca^{2+} \rightleftharpoons Ca(II)Pu(IV)(OH)_3ISA_{-2H}(aq) + 5\ H^+$	–(12.70 ± 0.08)

Table A4
SIT ion interaction coefficients of aqueous species in NaCl media.

Species i	Species j	$\varepsilon(i,j)$ [kg·mol^{-1}]	Reference
H^+	Cl^-	0.12 ± 0.01	Guillaumont et al. (2003)
Na^+	Cl^-	0.03 ± 0.01	Guillaumont et al. (2003)
Na^+	OH^-	0.04 ± 0.01	Guillaumont et al. (2003)
Na^+	ISA^-	-0.07 [a]	Colàs et al. (2011)
Ca^{2+}	Cl^-	0.14 ± 0.01	Guillaumont et al. (2003)
Pu^{4+}	Cl^-	0.4 ± 0.1	Neck and Kim (2001)
$PuOH^{3+}$	Cl^-	0.2 ± 0.1	Neck and Kim (2001)
$Pu(OH)_2^{2+}$	Cl^-	0.1 ± 0.1	Neck and Kim (2001)
$Pu(OH)_3^+$	Cl^-	0.05 ± 0.1	Neck and Kim (2001)
$Pu(OH)_4^0(aq)$	Na^+/Cl^-	0.00	[b]
$Pu(IV)(OH)_3ISA_{-H}^-$	Na^+	$-(0.05 \pm 0.10)$	[c]
$Pu(IV)(OH)_3ISA_{-2H}^{2-}$	Na^+	$-(0.10 \pm 0.10)$	[c]
$Pu(III)(OH)ISA_{-H}(aq)$	Na^+/Cl^-	0.00	[b]
$Ca(II)Pu(IV)(OH)_4ISA^+$	Cl^-	$-(0.05 \pm 0.10)$	[c]
$Ca(II)Pu(IV)(OH)_5ISA^0(aq)$	Cl^-/Na^+	0.00	[b]

[a] In analogy with $\varepsilon(Na+, Hox^-)$ reported in (Rand et al., 2009).
[b] By definition in SIT.
[c] Reported in (Tasi et al., 2018a, b), values are based on the work of Hummel (2009).

References

Aggarwal, S., Angus, M.J., Ketchen, J., 2000. Sorption of Radionuclides onto Specific Mineral Phases Present in Repository Cements. NSS/R312.

Altmaier, M., Neck, V., Fanghanel, T., 2008. Solubility of Zr(IV), Th(IV) and Pu(IV) hydrous oxides in CaCl2 solutions and the formation of ternary Ca-M(IV)-OH complexes. Radiochim. Acta 96.

Banik, N.L., Marsac, R., Lutzenkirchen, J., Diascorn, A., Bender, K., Marquardt, C.M., Geckeis, H., 2016. Sorption and redox speciation of plutonium at the illite surface. Environ. Sci. Technol. 50, 2092–2098.

Baston, G.M.N., Berry, J.A., Brownsword, M., Heath, T.G., Tweed, C.J., Williams, S.J., 1995. Sorption of plutonium and americium on repository, backfill and geological materials relevant to the JNFL low-level radioactive waste repository at Rokkasho-Mura. Mater. Res. Soc. Symp. Proc. 353, 957–964.

Bayliss, S., Howse, R.M., McCrohon, R., Oliver, P., 2000. Near-field Sorption Studies.

Bayliss, S., McCrohon, R., Oliver, P., Pilkington, N.J., Thomason, H.P., 1996. Near-field Sorption Studies: January 1989 to June 1991. NSS/R277.

Blanc, P., Bourbon, X., Lassin, A., Gaucher, E.C., 2010. Chemical model for cement-based materials: temperature dependence of thermodynamic functions for nanocrystalline and crystalline C–S–H phases. Cement Concr. Res. 40, 851–866.

Brendebach, B., Banik, N.L., Marquardt, C.M., Rothe, J., Denecke, M., Geckeis, H., 2009. X-ray absorption spectroscopic study of trivalent and tetravalent actinides in solution at varying pH values. Radiochim. Acta 97, 701–708.

Bruno, J., Gonzàles-Siso, M.R., Duro, L., Gaona, X., Altmaier, M., 2018. Key Master Variables Affecting the Mobility of Ni, Pu, Tc and U in the Near Field of the SFR Repository. Svensk Karnbranslehantering AB, Stockholm, Sweden. SKB Technical Report.

Ciavatta, L., 1980. The specific interaction theory in evaluating ionic equilibria. Ann. Chim. (Rome) 70, 551–567.

Colàs, E., Grivé, M., Rojo, I., Duro, L., 2011. Solubility of ThO2·xH2O(am) in the presence of gluconate. Radiochim. Acta 99, 269–273.

Duro, L., Domènech, C., Grivé, M., Roman-Ross, G., Bruno, J., Kallstrom, K., 2014. Assessment of the evolution of the redox conditions in a low and intermediate level nuclear waste repository (SFR1, Sweden). Appl. Geochem. 49, 192–205.

Evans, N., 2003. Studies on Metal α-Isosaccharinic Acid Complexes. Loughborough University, Loughborough, UK.

Fellhauer, D., 2013. Untersuchungen zur Redoxchemie und Loslichkeit von Neptunium und Plutonium, PhD-thesis. Ruprecht-Karls-Universitat Heidelberg, Heidelberg, Germany.

Gaona, X., Dahn, R., Tits, J., Scheinost, A.C., Wieland, E., 2011. Uptake of Np(IV) by C-S-H phases and cement paste: an EXAFS study. Environ. Sci. Technol. 45, 8765–8771.

Gaona, X., Montoya, V., Colàs, E., Grivé, M., Duro, L., 2008. Review of the complexation of tetravalent actinides by ISA and gluconate under alkaline to hyperalkaline conditions. J. Contam. Hydrol. 102, 217–227.

Glaus, M.A., Van Loon, L.R., 2008. Degradation of cellulose under alkaline conditions: new insights from a 12 years degradation study. Environ. Sci. Technol. 42, 2906–2911.

Glaus, M.A., Van Loon, L.R., Achatz, S., Chodura, A., Fischer, K., 1999. Degradation of cellulosic materials under the alkaline conditions of a cementitious repository for low and intermediate level radioactive waste. Part I: identification of degradation products. Anal. Chim. Acta 398, 111–112.

Greenfield, B.F., Hurdus, M.H., Spindler, M.W., Thomason, H.P., 1997. The Effect of the Products from the Anaerobic Degradation of Cellulose on the Solubility and Sorption of Radioelements in the Near Field. Nuclear Industry Radioactive Waste Executive (Nirex), UK.

Guillaumont, R., Fanghanel, T., Neck, V., Fuger, J., Palmer, D.A., Grenthe, I., Rand, M.H., 2003. Update on the Chemical Thermodynamics of Uranium, Neptunium, Plutonium, Americium and Technetium. Elsevier, North Holland, Amesterdam.

Holgersson, S., Albinsson, Y., Allard, B., Borén, H., Pavasars, I., Engkvist, I., 1998. Effects of gluco-isosaccharinate on Cs, Ni, Pm and Th sorption onto, and diffusion into cement. Radiochim. Acta 82, 393–398.

Hummel, W., 2009. Ionic Strength Corrections and Estimation of SIT Ion Interaction Coefficients, PSI Technical Report. Paul Scherrer Institut, Villigen, Switzerland.

Hummel, W., Anderegg, G., Rao, L., Puigdomenech, I., Tochiyama, O., 2005. Chemical Thermodynamics of Compounds and Complexes of U, Np, Pu, Am, Tc, Se, Ni and Zr with Selected Organic Ligands. Elsevier, North-Holland, Amsterdam.

Kinniburgh, D.G., Cooper, D.M., 2009. PhreePlot: Creating Graphical Output with PHREEQC. Centre for Ecology and Hydrology, Deiniol Road, Bangor, Gwynedd, LL57 2UW, UK.

Marsac, R., Banik, N.l., Lützenkirchen, J., Marquardt, C.M., Dardenne, K., Schild, D., Rothe, J., Diascorn, A., Kupcik, T., Schafer, T., Geckeis, H., 2015. Neptunium redox speciation at the illite surface. Geochem. Cosmochim. Acta 152, 39–51.

Moreton, A.D., 1993. Thermodynamic modeling of the effect of hydroxycarboxylic acids on the solubility of plutonium at high pH. Mater. Res. Soc. Symp. Proc. 294, 753–758.

Moreton, A.D., Pilkington, N.J., Tweed, C.J., 2000. Thermodynamic Modeling of the Effect of Hydroxycarboxylic Acids on the Solubility of Plutonium at High pH. Nuclear Industry Radioactive Waste Executive (Nirex), UK.

Neck, V., Altmaier, M., Fanghanel, T., 2007. Solubility of plutonium hydroxides/hydrous oxides under reducing conditions and in the presence of oxygen. Compt. Rendus Chem. 10, 959–977.

Neck, V., Kim, J.I., 2001. Solubility and hydrolysis of tetravalent actinides. Radiochim. Acta 89, 1–16.

Ochs, M., Mallants, D., Wang, L., 2016. Radionuclide and Metal Sorption on Cement and Concrete. Springer International Publishing, Switzerland.

Parkhurst, D.L., Appelo, C.A.J., 1999. User's Guide to PHREEQC (Version 2) – a Computer Program for Speciation, Batch Reaction, One-Dimensional Transport and Inverse Geochemical Calculation, Water-Resources Investigation Report 99–4259. USGS, Denver, Colorado, USA, p. 312.

Parkhurst, D.L., Appelo, C.A.J., 2013. Description of input and examples for PHREEQC version 3—a computer program for speciation, batch-reaction, one-dimensional transport, and inverse geochemical calculations: U.S. Geological Survey Techniques and Methods. available only at: http://pubs.usgs.gov/tm/06/a43/.

Pointeau, I., Coreau, N., Reiller, P.E., 2008. Uptake of anionic radionuclides onto degraded cement pastes and competing effect of organic ligands. Radiochim. Acta 96.

Pointeau, I., Hainos, D., Coreau, N., Reiller, P., 2006a. Effect of organics on selenite uptake by cementitious materials. Waste Manag. 26 (7), 733–740.

Pointeau, I., Landesman, C., Coreau, N., Moisan, C., Reiller, P., 2004. Etude de la rétention chimique des radionucléides Cs(I), Am(III), Zr(IV), Pu(IV), Nb(V), U(VI) et Tc(IV) par les matériaux cimentaires dégradés. CEA report 2004.

Pointeau, I., Reiller, P., Mace, N., Landesman, C., Coreau, N., 2006b. Measurement and modeling of the surface potential evolution of hydrated cement pastes as a function of degradation. J. Colloid Interface Sci. 300, 33–44.

Rai, D., Hess, N.J., Xia, Y.X., Rao, L., Cho, H.M., Moore, R.C., Van Loon, L.R., 2003. Comprehensive thermodynamic model applicable to highly acidic to basic conditions for isosaccharinate reactions with Ca(II) and Np(IV). J. Solut. Chem. 32, 665–689.

Rai, D., Kitamura, A., 2015. Evaluation of equilibrium constants for deprotonation and lactonisation of α-D-isosaccharinic acid. J. Nucl. Sci. Technol. 53, 459–467.

Rai, D., Kitamura, A., 2017. Thermodynamic equilibrium constants for important isosaccharinate reactions: a review. J. Chem. Therm. 114, 135–143.

Rand, M., Fuger, J., Grenthe, I., Neck, V., Rai, D., 2009. Chemical Thermodynamics of Thorium. Elsevier, North-Holland, Amsterdam.

Ravel, B., Newville, M., 2005. ATHENA, ARTEMIS, HEPHAESTUS: data analysis for X-ray absorption spectroscopy using IFEFFIT. J. Synchrotron Radiat. 12, 537–541.

Rojo, H., Tits, J., Gaona, X., Garcia-Gutiérrez, M., Missana, T., Wieland, E., 2013. Thermodynamics of Np(IV) complexes with gluconic acid under alkaline conditions: sorption studies. Radiochim. Acta 101, 133–138.

Rothe, J., Butorin, S., Dardenne, K., Denecke, M.A., Kienzler, B., Loble, M., Metz, V., Seibert, A., Steppert, M., Vitova, T., Walther, C., Geckeis, H., 2012. The INE-Beamline for actinide science at ANKA. Rev. Sci. Instrum. 83, 043105.

Schepperle, J., 2020. Untersuchungen zur Loslichkeit und Komplexierung von vierwertigem Plutonium und Neptunium in verdünnten und konzentrierten Salzlosungen, PhD-thesis. Institute for Nuclear Waste Disposal (INE). Karlsruhe Institute of Technology, Karlsruhe, Germany.

Schubert, J., 1948. The use of ion exchangers of the determination of physical-chemical properties of substances, particularly radiotracers, in solution. I. Theoretical. J. Phys. Colloid Chem. 52, 340–350.

Scrivener, K., Snellings, R., Lothenbach, B., 2016. A Practical Guide to Microstructural Analysis of Cementitious Materials. CRC Press, Taylor & Francis Group, Boca Raton, FL (USA).

Seah, M.P., Gilmore, L.S., Beamson, G., 1998. XPS: binding energy calibration of electron spectrometers 5 - Re-evaluation of the reference energies. Surf. Interface Anal. 26, 642–649.

Siretanu, I., Ebeling, D., Andersson, M.P., Stipp, S.L., Philipse, A., Stuart, M.C., van den Ende, D., Mugele, F., 2014. Direct observation of ionic structure at solid-liquid interfaces: a deep look into the Stern Layer. Sci. Rep. 4, 4956.

SKB, 2008. Safety Analysis SFR 1. Long-Term Safety. Svensk Karnbranslehantering AB, Stockholm, Sweden.

Tasi, Á., Gaona, X., Fellhauer, D., Bottle, M., Rothe, J., Dardenne, K., Polly, R., Grive, M., Colas, E., Bruno, J., Kallstrom, K., Altmaier, M., Geckeis, H., 2018a. Thermodynamic description of the plutonium - alpha-D-isosaccharinic acid system I: solubility, complexation and redox behavior. Appl. Geochem. 98, 247–264.

Tasi, Á., Gaona, X., Fellhauer, D., Bottle, M., Rothe, J., Dardenne, K., Polly, R., Grive, M., Colas, E., Bruno, J., Kallstrom, K., Altmaier, M., Geckeis, H., 2018b. Thermodynamic description of the plutonium - alpha-D-isosaccharinic acid system II: formation of quaternary Ca(II)-Pu(IV)-OH-ISA complexes. Appl. Geochem. 98, 351–366.

Tasi, Á., Gaona, X., Fellhauer, D., Bottle, M., Rothe, J., Dardenne, K., Schild, D., Grive, M., Colas, E., Bruno, J., Kallstrom, K., Altmaier, M., Geckeis, H., 2018c. Redox behavior and solubility of Plutonium under alkaline, reducing conditions. Radiochim. Acta 106, 259–279.

Tits, J., Fujita, T., Harfouche, M., Dahn, R., Tsukamoto, M., Wieland, E., 2014a. Radionuclide Uptake by Calcium Silicate Hydrates: Case Studies with Th(IV) and U (VI), PSI-Bericht. Paul Scherrer Institut, CH-5232 Villigen PSI, Switzerland.

Tits, J., Gaona, X., Laube, A., Wieland, E., 2014b. Influence of the redox state on the neptunium sorption under alkaline conditions: batch sorption studies on titanium dioxide and calcium silicate hydrates. Radiochim. Acta 102.

Tits, J., Wieland, E., 2018. Actinide Sorption by Cementitious Materials, PSI Bericht. Paul Scherrer Institut, CH-5232 Villigen PSI, Switzerland.

Tits, J., Wieland, E., Bradbury, M.H., 2005. The effect of isosaccharinic acid and gluconic acid on the retention of Eu(III), Am(III) and Th(IV) by calcite. Appl. Geochem. 20, 2082–2096.

Tits, J., Wieland, E., Bradbury, M.H., Eckert, P., Schaible, A., 2002. The Uptake of Eu(III) and Th(IV) by Calcite under Hyperalkaline Conditions. Paul Scherrer Insitut, Villigen, Switzerland.

Tits, J., Wieland, E., Muller, C.J., Landesman, C., Bradbury, M.H., 2006. Strontium binding by calcium silicate hydrates. J. Colloid Interface Sci. 300, 78–87.

Van Loon, L.R., Glaus, M.A., 1998. Experimental and Theoretical Studies on Alkaline Degradation of Cellulose and its Impact on the Sorption of Radionuclides. Paul Scherrer Institute, Switzerland.

Van Loon, L.R., Glaus, M.A., Stallone, S., Laube, A., 1997. Sorption of isosaccharinic acid, a cellulose degradation product, on cement. Environ. Sci. Technol. 31, 1243–1245.

Vercammen, K., 2000. Complexation of Calcium, Thorium and Europium by α-Isosaccharinic Acid under Alkaline Conditions. Swiss Federal Institute of Technology, Zurich, Switzerland.

Vercammen, K., Glaus, M.A., Van Loon, L.R., 2001. Complexation of Th(IV) and Eu(III) by alpha-isosaccharinic acid under alkaline conditions. Radiochim. Acta 89, 393–401.

Walther, C., Rothe, J., Brendebach, B., Fuss, M., Altmaier, M., Marquardt, C.M., Büchner, S., Cho, H.-R., Yun, J.I., Seibert, A., 2009. New insights in the formation processes of Pu(IV) colloids. Radiochim. Acta 97, 199–207.

Wang, L., Martens, E., Jacques, D., De Cannière, P., Berry, J., Mallants, D., 2009. Review of Sorption Values for the Cementitious Near Field of a Near Surface Radioactive Waste Disposal Facility. ONDRAF/NIRAS, Brussels, Belgium.

Wieland, E., 2014. Sorption Data Base for the Cementitious Near Field of L/ILW and ILW Repositories for Provisional Safety Analyses for SGT-E2, NAGRA Technical Report. Paul Scherrer Institut, Wettlingen, Switzerland.

Wieland, E., Tits, J., Dobler, J.P., Spieler, P., 2002. The effect of α-isosaccharinic acid on the stability of and Th(IV) uptake by hardened cement paste. Radiochim. Acta 90, 683–688.

Repository KITopen

Dies ist ein Postprint/begutachtetes Manuskript.